Optimal Model Reduction and Robust Feedback Control for Aerodynamics

AFoSR Grant AF-FA9550-08-1-0450

Seddik M. Djouadi
Department of Electrical Engineering and Computer Science
University of Tennessee, Knoxville, TN 37922-2100
djouadi@eecs.utk.edu

Abstract

In this project, methods of model reduction that integrate feedback active flow control with applications to nonlinear convection and turbulent flows governed by Navier-Stokes equations are developed. A new methodology which extracts boundary conditions in reduced order proper orthogonal decomposition (POD) and finite difference models is developed. A new model reduction method based on empirical data and balanced truncation was developed and applied to nonlinear Galerkin models. Based on this method a new empirical Hankel norm model reduction algorithm is proposed. These methods are applied to a prototype nonlinear convective problem governed by the two-dimensional (2D) Burgers' equation. The reduced models are used in the design of robust boundary controllers that achieve tracking, and implemented on the full order Computational Fluid Dynamics (CFD) models.

POD and balanced truncation are shown to be optimal in the sense of distance minimizations in spaces of Hilbert-Schmidt (HS) operators. POD has been shown to be optimal in a broader sense than is reported in the literature. The optimality is in the sense of distance minimization in a space of integral operators under the Hilbert-Schmidt norm. A connection with balanced truncation is found. In particular, balanced truncation is shown to be optimal in the sense of distance minimization albeit in a different space of integral operators under the Hilbert-Schmidt norm when the so-called 'Curtain-Glover' balanced realization is used. This is a novel discovery as balanced truncation is usually known to be not optimal in any sense.

An algorithm that combines the extended Kalman filter and expectation maximization to estimate the model coefficients from particle image velocimetry (PIV) measurements for turbulent 2D flows is developed. The algorithm is recursive and convenient for on-line implementation. The method is applied to a 2D flow control problem over the NACA 4412 airfoil using experimental data obtained from Prof. Glauser's flow control group at the University of Syracuse. The motivation for this problem is minimization of aero-optic distortion in a bluff-body flow.

POD and balanced truncation are shown to minimize different n-widths of partial differential equation solutions including the Kolmogorov, Gelfand, linear and Bernstein n-widths. The n-widths are notions from metric complexity theory. They quantify inherent and representation errors due to lack of data and loss of information.

Report Documentation Page

Form Approved
OMB No. 0704-0188

1. REPORT DATE	2. REPORT TYPE	3. DATES COVERED
29 MAR 2010	**Final**	**01-08-2008 to 30-06-2010**

4. TITLE AND SUBTITLE	5a. CONTRACT NUMBER
OPTIMAL MODEL REDUCTION AND ROBUST FEEDBACK CONTROL FOR AERODYNAMICS	**FA9550-08-1-0450**
	5b. GRANT NUMBER
	5c. PROGRAM ELEMENT NUMBER
6. AUTHOR(S) **Seddik Djouadi**	5d. PROJECT NUMBER
	5e. TASK NUMBER
	5f. WORK UNIT NUMBER
7. PERFORMING ORGANIZATION NAME(S) AND ADDRESS(ES) **Department of Electrical Engineering and Computer Science,University of Tennessee,Knoxville ,TN,37922-2100**	8. PERFORMING ORGANIZATION REPORT NUMBER **; AFRL-OSR-VA-TR-2011-0220**
9. SPONSORING/MONITORING AGENCY NAME(S) AND ADDRESS(ES) **AFOSR, 875 North Randolph Street, Suite 325, Arlington, VA, 22203**	10. SPONSOR/MONITOR'S ACRONYM(S)
	11. SPONSOR/MONITOR'S REPORT NUMBER(S) **AFRL-OSR-VA-TR-2011-0220**

12. DISTRIBUTION/AVAILABILITY STATEMENT
Approved for public release; distribution unlimited

13. SUPPLEMENTARY NOTES

14. ABSTRACT

In this project, methods of model reduction that integrate feedback active flow control with applications to nonlinear convection and turbulent flows governed by Navier-Stokes equations are developed. A new methodology which extracts boundary conditions in reduced order proper orthogonal decomposition (POD) and finite difference models is developed. A new model reduction method based on empirical data and balanced truncation was developed and applied to nonlinear Galerkin models. Based on this method a new empirical Hankel norm model reduction algorithm is proposed. These methods are applied to a prototype nonlinear convective problem governed by the two-dimensional (2D) Burgers? equation.

15. SUBJECT TERMS

16. SECURITY CLASSIFICATION OF:			17. LIMITATION OF ABSTRACT	18. NUMBER OF PAGES	19a. NAME OF RESPONSIBLE PERSON
a. REPORT **unclassified**	b. ABSTRACT **unclassified**	c. THIS PAGE **unclassified**	**Same as Report (SAR)**	**55**	

Most model reduction algorithms assume linear models and fail when applied to nonlinear high dimensional systems, in particular, fluid flow problems with elevated Reynolds numbers. For example, POD fails to capture the nonlinear degrees of freedom in these systems, since it assumes that data belong to a linear space and therefore relies on the Euclidean distance as the metric to minimize. However, snapshots generated by nonlinear PDEs belong to manifolds for which the geodesics, when they exist, do not correspond in general to the Euclidean distance. A geodesic is a curve that is locally the shortest path between two points. We propose a model reduction method which generalizes POD to nonlinear fluid flows corresponding to manifolds which have a differentiable structure at each of their points. The algorithm is applied to a prototype nonlinear turbulent flow on the Wortmann FX 60-100 airfoil governed by the Navier-Stokes equation.

I. Introduction

Recent advances in actuators, sensors, simulation, and experimental diagnostics bring applications such as suppression of acoustic tones in cavities, separation control for high lift, and trajectory control without moving hinged surfaces within reach. However, these applications require the integration of feedback control because of the need for robustness to flight condition and vehicle attitude, precision tracking, overcoming low-fidelity models, or moving a system away from a stable solution or limit cycle as efficiently as possible. Feedback control strategies in which the bandwidth of the controller is commensurate with the time scales of fluid flows are attractive because they offer the possibility of improved performance and reduced control power required through control of unstable structures in the flow field. Unfortunately, models that capture the relevant dynamics of the input-output system and are amenable to control design are difficult to develop [1].

There has been significant interest in model reduction for the purpose of control design [2][3][4][5][6][7][8][9][10]. One such application of reduced order modeling is control design in the context of aerodynamic flow. Aerodynamic flow control is a research area of great interest to the Air Force and the fluid mechanics community. Presently considerable research efforts are working with feedback control law design for systems described by PDEs that need a very large number of states to accurately simulate their characteristics. However, recent advances in the design of actuators and sensors can be leveraged for better system control only if the control design methods provide a reliable low order controller [11]. Additionally, simulation, and experimental diagnostics are making applications such as the suppression of acoustic tones in cavities, separation control for high lift, and trajectory control without the need to move hinged surfaces a possibility [12]. However, these applications require the integration of feedback control because of the need for robustness to flight condition and vehicle attitude, precision tracking overcoming low-fidelity models, or moving a system away from a stable solution or limit cycle as efficiently as possible [12].

Unfortunately, it is very difficult to create models that capture the relevant dynamics of the input-output system. For example, computational fluid dynamics simulations can provide good solutions to a discretized version of the Navier-Stokes equation [2], [13]. However, accurate simulations for simple shapes such as two-dimensional airfoils, or complex shapes, such as a full vehicle, require several thousands to millions of states. Therefore, the simulation results are not

directly useful for control design [12]. Complexity in the model is a legitimate need. The large number of states is necessary to capture important flow features that occur at extremely small spatial scales. Although these small flow features might seem insignificant, if they are not captured, it is not possible to analyze if they are necessary in securing the closed loop system's overall stability [11].

POD has been extensively investigated in distributed parameters systems due to its order reduction capability [8][9][10][14][15], and balanced truncation, which is a simple yet efficient model reduction technique widely used in reducing model orders of high order linear systems [16][18][19]. POD models of only a few dozen states can often accurately capture the input-output behavior of systems that have full order system models of thousands of states [12]. In addition to using the POD method in conjunction with model reduction techniques, the idea of using empirical gramians is growing in popularity for use in an approximate balanced truncation [20][5] [21][17]. Further, some work has been done on finding nonlinear empirical gramians for balanced truncation [22][23].

In fluid flow configurations it is not uncommon for discretized flow models to describe thousands to millions of state variables, for example if one uses a linear quadratic regulator (LQR) control formulation, roughly 10^{12} Riccati unknowns need to be calculated for a discretized flow model describing 10^{6} states. Existing computing power and computational algorithms are not capable of solving an LQR problem of such large dimension. For dynamical models that are very large scale, such as those describing fluid flow configurations, it is apparent that the order of the system must be reduced prior to control law design [24]. This prevents us from using closed loop model reduction strategy wherein the system is part of a closed loop system with a controller [25].

In the area of fluid mechanics controls must often be fixed to the boundary of the problem geometry. For example, control of flow separation over an airfoil requires that actuation and sensing be done on the airfoil surface [12]. The problem geometry used for this project is one example of a case where control is restricted to the boundaries by physical necessity.

The rest of the report is organized as follows. In section II, POD is shown to be optimal in a more general sense to what is reported in the literature. In particular, POD is shown to be optimal in the sense of distance minimizations in space of Hilbert- Schmidt or trace-class 2 integral operators. In section III, balanced truncation is shown to be optimal in terms of approximation by finite rank operators in the Hilbert-Schmidt norm when the Curtain-lover balanced realization is used. In section IV, a prototype nonlinear convection problem is introduced. A new empirical balanced truncation is developed in sections V and VI. The method is applied to nonlinear convection in section VII. A new empirical Hankel norm model reduction is developed and applied to the nonlinear convection prototype problem in sections VIII and IX, respectively. In section X a H^{∞} flow controller that achieve tracking for the nonlinear convective flow is designed based on the reduce order models and applied to the full order system. In section XI, model estimation and identification algorithms that combine the Kalman filter and expectation maximization for POD modes of a turbulent flow over the NACA 4412 airfoil are presented. In section XII, POD and balanced truncation are related to metric complexity theory with the notion

of n-with approximation. In section XIII, a generalization of POD to nonlinear PDEs using the notion of auto-associative models is proposed. Section XIV contains concluding remarks.

II. Optimality of the Proper Orthogonal Decomposition (POD)

POD has been used extensively to determine efficient bases for dynamical systems, random processes and large data set in general. It was introduced in the context of turbulence by Lumley [26]. It is also known as the Karhunen-Loeve decomposition, principal component analysis, singular systems analysis, and singular value decomposition [27][28]. The fundamental idea behind POD is as follows: Given a set of simulation/experimental data or snapshots $\{S_i\}_{i=1}^{N}$ of a function $w(t,\mathrm{x})$, in the standard Hilbert space $L^2([0,T)\times\Omega)$, where $\mathbf{x}\in\Omega$ for some set (spatial domain) Ω of $\mathbb{R}^p$ and T represents a finite or infinite time interval. The n-th POD vector $\phi_n(\mathbf{x})$ is chosen recursively so as to minimize the cost function [26][29]

$$J(\phi_n) := \int_{[0,T)}\int_{\Omega} | S_i(t,\mathrm{x}) - \sum_{j=1}^{n} \alpha_i \phi_i(\mathrm{x}) |^2 \, d\mathrm{x}dt \tag{1}$$

subject to the constraints

$$\alpha_j(t) = \int_{\Omega} S_i(t,\mathbf{x})\,\phi_j(\mathbf{x})\,d\mathbf{x} \tag{2}$$

$$\int_{\Omega} \phi_i(\mathbf{x})\,\phi_j(\mathbf{x})\,d\mathbf{x} = \delta_{ij}, \text{ for } i,\, j = 1, 2, \cdots, n \tag{3}$$

The optimal POD basis is given by the eigenfunctions $\{\phi_i(\mathrm{x})\}$ of the averaged autocorrelation function, denoted $R(\mathrm{x},\mathrm{x}')$, of the snapshots, that is, [26][27]

$$R(\mathbf{x},\mathbf{x}') = \int_{[0,T)} S_i(t,\mathbf{x})\, S_i(t,\mathbf{x}')\, dt \tag{4}$$

which solves the eigenvalue problem

$$\int_{\Omega}\int_{[0,T)} S_i(t,\mathbf{x})\, S_i(t,\mathbf{x}')\,\phi(\mathbf{x}')dtd\mathbf{x} = \lambda\phi(\mathbf{x}) \tag{5}$$

The Hilbert space $L^2([0,T)\times\Omega)$ is endowed with the norm

$$\|w(t,\mathbf{x})\|_2 := \left(\int_{[0,t)}\int_{\Omega} |w(t,\mathbf{x})|^2 \, d\mathbf{x}dt \right)^{\frac{1}{2}} \tag{6}$$

Define the shortest distance minimization in the $\|\cdot\|_2$-norm from the function $w(t,\mathbf{x})$ to the subspace S, by

$$\mu := \inf_{s\in S} \|w(t,\mathbf{x}) - s(t,\mathbf{x})\|_2 \tag{7}$$

where the subspace S is defined as

$$S := \left\{ \sum_{k=1}^{n} \alpha_k(t)\,\phi_k(\mathrm{x}),\ \alpha_k(t)\in L^2([0,T)),\ \phi_k(\mathrm{x})\in L^2(\Omega),\ n \text{ integer} \right\} \tag{8}$$

Note that this distance problem is posed in an infinite dimensional space. For finite dimensional spaces, in particular for distances to lower rank matrices see [30], where SVD techniques are

used. To compute the distance we view $w(t,\mathbf{x})$ as a Hilbert- Schmidt kernel for an integral operator T mapping $L^2(\Omega)$ into $L^2([0,T))$ both endowed with the standard $\|\cdot\|_2$-norm, and defined by

$$(T\phi)(t) := \int_{\Omega} w(t,\mathbf{x})\phi(\mathbf{x})d\mathbf{x} \tag{9}$$

It is known that such an operator is compact [31], that is, an operator which maps bounded sets into pre-compact sets. The operator T is said to be a Hilbert-Schmidt or a trace-class 2 operator [32]. Let us denote the class of Hilbert-Schmidt operators acting from $L^2([0,T))$ into $L^2(\Omega)$, by C_2, and the Hilbert-Schmidt norm $\|\cdot\|_{\mathrm{HS}}$.

Define the adjoint of T by T^* as the operator acting from $L^2([0,T))$ into $L^2(\Omega)$ by

$$\begin{aligned} <Tf, g>_2 &:= \int_{[0,T)}\int_{\Omega} w(t,\mathbf{x}) f(\mathbf{x})d\mathbf{x}g(t)dt \\ &= \int_{\Omega} f(\mathbf{x}) \int_{[0,T)} w(t,\mathbf{x})g(t)dtd\mathbf{x} \end{aligned} \tag{10}$$

$$=: <f, T^*g>_1 \tag{11}$$

showing that $(T^*g)(t) = \int_{[0,T)} w(t,\mathbf{x})g(t)dt$.

Using the polar representation of compact operators [32], $T = U(T^*T)^{1/2}$, where U is a partial isometry and $(T^*T)^{1/2}$ the square root of T, which is also a Hilbert-Schmidt operator, and admits a spectral factorization of the form [32]

$$(T^*T)^{1/2} = \sum_i \lambda_i v_i \otimes v_i \tag{12}$$

where $\lambda_i > 0$, $\lambda_i \searrow 0$ as $i \uparrow \infty$, are the eigenvalues of $(T^*T)^{1/2}$, and v_i form the corresponding orthonormal sequence of eigenvectors, i.e., $(T^*T)^{1/2} v_i = \lambda_i v_i$, $i = 1,2,\cdots$. Putting $Uv_i =: \varphi_i$, we can write

$$T = \sum_i \lambda_i v_i \otimes \varphi_i \tag{13}$$

Both $\{v_i\}$ and $\{\varphi_i\}$ are orthonormal sequences in $L^2([0,T))$ and $L^2(\Omega)$, respectively. The sum (13) has either a finite or countably infinite number of terms. The above representation is unique.

Noting that the polar decomposition of $T^* = U^*(TT^*)^{1/2}$, a similar argument yields

$$(TT^*)^{\frac{1}{2}} = \sum_i \lambda_i \varphi_i \otimes \varphi_i \tag{14}$$

$$T^* = \sum_i \lambda_i \varphi_i \otimes v_i \tag{15}$$

which shows that α_i form an orthonormal sequence of eigenvectors of $(TT^*)^{1/2}$ corresponding to the eigenvalues λ_i. From (12) and (15) it follows that

$$T\varphi_i = U(T^*T)^{1/2}\varphi_i = \lambda_i v_i \tag{16}$$

$$Tv_i = U(TT^*)^{\frac{1}{2}} v_i = \lambda_i \varphi_i \tag{17}$$

We say that φ_i and v_i constitute a Schmidt pair [31]. In terms of integral operators expressions, identities (16) and (17) can be written, respectively, as

$$v_i(t) = \int_{\Omega} w(t,\mathbf{x})\varphi_i(\mathbf{x})d\mathbf{x} \tag{18}$$

$$\varphi_i(t) = \int_{0}^{T} w(t,\mathbf{x})v_i(t)dt \tag{19}$$

In terms of the eigenvalues λ_i's of *T*, its Hilbert-Schmidt norm $\|.\|_{HS}$ is given by [32]

$$\|T\|_{HS} = \left(\sum_i \lambda_i^2\right)^{\frac{1}{2}} = \left(\int_0^T \int_{\Omega} |w(t,\mathbf{x})|^2 \, d\mathbf{x}dt\right)^{\frac{1}{2}} \tag{20}$$

Note that since the operator *T* is Hilbert-Schmidt the sum in (20) is finite. The Hilbert-Schmidt norm is also induced by the operator inner product defined by (23).

By interpreting each elements of the subspace *S* defined in (8) as a Hilbert-Schmidt operator as we did for $w(t,\mathbf{x})$ we see that *S* is the subspace of Hilbert-Schmidt operators of rank *n*, i.e.,

$$S = \{s = \sum_{j=1}^{n} \vartheta_j f_j(t) \otimes \chi_j(\mathbf{x}) : f_j(t) \in L^2(T),\ \chi_j(\mathbf{x}) \in L^2(\Omega), \vartheta_i \in \mathbb{R}\} \tag{21}$$

In addition, the distance minimization (7) is then the minimal distance from *T* to Hilbert-Schmidt operators of rank *n*. In other terms, we have

$$\mu = \min_{s \in S} \|T - s\|_{HS} \tag{22}$$

The space of Hilbert-Schmidt operators is in fact a Hilbert space with the inner product [32], denoted $(\cdot,\cdot)$, if *A* and *B* are two Hilbert-Schmidt operators defined on $L^2(\Omega)$,

$$(A,B) := tr(B^*A) \tag{23}$$

where *tr* denotes the trace, which in this case is given by the sum of the eigenvalues of the operator B^*A which is necessarily finite [32]. Note that the inner product (23) induces the Hilbert-Schmidt norm $\|A\|_{HS} = \left(tr\left(A^*A\right)\right)^{1/2}$.

In the case where *A* and *B* are integral operators with kernels $A(t,\mathbf{x})$ and $B(t,\mathbf{x})$, respectively, the inner product can be realized concretely by

$$(A,B) = \int_0^T \int_{\Omega} A(t,\mathbf{x})B(t,\mathbf{x})d\mathbf{x}dt \tag{24}$$

The solution to the distance minimization (22) is simply given by the orthogonal projection of T onto S. To compute the latter, note that the eigenvectors of $\left(TT^*\right)^{1/2}$ and $\left(T^*T\right)^{1/2}$ form orthonormal bases (by completing them if necessary) for $L^2([0,T))$ and $L^2(\Omega)$, respectively. In terms of the eigenvectors v_j and φ_j the subspace S can be written as

$$S = Span\{v_j \otimes \varphi_j,\ j = 1,2,\cdots,n\} \tag{25}$$

Since the shortest distance minimization (22) is posed in a Hilbert space, by the principle of orthogonality it is solved by the orthogonal projection P_S acting from C_2 onto S. The latter can be computed by first determining the orthogonal projection P_v onto $Span\{v_j,\ j = 1,2,\cdots,n\}$, and the orthogonal projection P_φ onto $Span\{\varphi_j,\ j = 1,2,\cdots,n\}$. These projections have finite rank and since the v_j and φ_j's are orthogonal vectors in $L^2([0,T))$ and $L^2(\Omega)$, respectively, it can be easily verified that P_v and P_φ are given by

$$\begin{aligned}
\left(P_v f\right)(t) &= \sum_{j=1}^{n} \left\langle f, v_j \right\rangle_1 v_j(t) = \sum_{j=1}^{n} \left(\int_0^T f(t) v_j(t) dt \right) v_j(t) \\
\left(P_\varphi G\right)(\mathbf{x}) &= \sum_{j=1}^{n} \left\langle G, \varphi_j \right\rangle_2 \varphi_j = \sum_{j=1}^{n} \left(\int_\Omega G(\mathbf{x}) \varphi_j(\mathbf{x}) d\mathbf{x} \right) \varphi_j(\mathbf{x})
\end{aligned} \tag{26}$$

The overall orthogonal projection P_S can be computed as

$$P_S = P_v \otimes P_\varphi \tag{27}$$

That is, if $W \in C_2$ has spectral decomposition $\sum_i \eta_i u_i \otimes v_j$, where $u_i \in L^2(T)$, $\vartheta_i \in L^2(\Omega)$ then

$$\begin{aligned}
P_S W &= \sum_{i=1} \eta_i P_S (u_i \otimes \vartheta_i) \\
&= \sum_{i=1} \eta_i \left(\sum_{j=1}^{n} \left(\int_0^T u_i(t) v_j(t) dt \right) v_j \otimes \left(\int_\Omega \left(\vartheta_i(\mathbf{x}) \varphi_j(\mathbf{x}) d\mathbf{x} \right) \varphi_j \right) \right) \\
&= \sum_{j=1}^{n} \theta_j v_j \otimes \varphi_j,\ \ \exists\ scalers\ \ \theta_j
\end{aligned} \tag{28}$$

where the last finite sum is obtained thanks to orthogonality, i.e., only the u_i's and ϑ_j's that live in the span of v_j's and φ_j's, respectively, are retained. For the orthogonality property we only need verify that

$$x \otimes y - (P_v \otimes P_\varphi)(x \otimes y) \perp u \otimes v,\ \ x \in L^2([0,T)),\ \ y \in L^2(\Omega),\ \ u \otimes v \in S$$

Computing the inner product, we get

$$< x - P_v x, u >_1 < y - P_\varphi, v >_2 = 0$$

Because P_v is the orthogonal projection of $L^2([0,T))$ onto $Span\{v_j,\ j = 1,2,\cdots,n\}$, and P_φ the orthogonal projection of $L^2(\Omega)$ onto $Span\{\varphi_j,\ j = 1,2,\cdots,n\}$. The minimizing operator $s_0 \in S$ in (22) is then given by

$$s_0 := P_S T = \sum_{i=1}^{n} \lambda_i v_i \otimes \varphi_i \tag{29}$$

and

$$\mu = \min_{s \in S} \left\| w(t,\mathbf{x}) - s(t,\mathbf{x}) \right\|_2 = \left\| T - P_S T \right\|_{HS} = \left(\sum_{i=n+1}^{\infty} \lambda_i^2 \right)^{1/2} \tag{30}$$

And as $n \uparrow \infty$, $\left\| T - P_S T \right\|_{HS} \searrow 0$. Therefore, the minimizing function $s_0(t,\mathbf{x})$ in (7) corresponds to the kernel of s_0, which is given by

$$s_0(t,\mathbf{x}) = \sum_{i=1}^{n} \lambda_i v_i(t) \varphi_i(\mathbf{x}) \tag{31}$$

Now note that $\alpha_i(t) = \lambda_i v_i(t)$, $\phi(\mathbf{x}) = \varphi(\mathbf{x})$, we see that $s_0(t,\mathbf{x})$ solves the optimization problem (1) since it minimizes the cost function $J(\phi_n)$ and $\alpha_i(t)$, $\phi_i(\mathbf{x})$ satisfy constraints (2) and (3), respectively. Moreover, (18) and (19) imply that $\phi_i(\mathbf{x})$ is related to $\alpha_i(t)$ by

$$\phi_i(\mathbf{x}) = \frac{1}{\lambda_i} \int_0^T w(t,\mathbf{x}) \alpha_i(t) dt \tag{32}$$

In the next section, we show that balanced truncation is in some sense similar to POD, in that, it is also optimal in the sense of distance minimization in the Hilbert-Schmidt norm, albeit in different operator spaces. The techniques developed for POD will help us in the context of showing the optimality of balanced truncation as well.

III. Optimality of Balanced Truncation

Balanced truncation is a simple and popular model reduction technique, which can be described as follows [21][18]: Suppose we have a stable linear time invariant (LTI) system described by the following *n*-dimensional state space equation

$$\begin{aligned} \dot{x}(t) &= Ax(t) + Bu(t) \\ y(t) &= Cx(t) \end{aligned} \tag{33}$$

where $x(t)$ is the $n \times 1$-state vector of the system, *u(t)* is an $m \times 1$-input vector, and *y*(*t*) is an $p \times 1$-output or measurement vector. *A*, *B*, and *C* are constant matrices of appropriate dimensions.

The underlying idea of balanced truncation is to take into account both the input and output signals of the system when deciding which states to truncate with appropriate scaling. The latter is performed by transforming the controllability and observability gramians, denoted W_c and W_o respectively, so that they are equal and diagonal.

The controllability and observability gramians satisfy the following Lypaunov equations [18]

$$AW_c + W_c A^T + BB^T = 0 \tag{34}$$

$$A^T W_o + W_o A + C^T C = 0 \tag{35}$$

The controllability and observability gramians can be represented as

$$W_c = \int_0^{\infty} e^{At} BB^T e^{A^T t} dt, \quad W_o = \int_0^{\infty} e^{A^T t} C^T C e^{At} dt$$

Computing a state balancing transformation M is achieved by first calculating the matrix [18,19], $W_{co} := W_c W_o$, and determining its eigenmodes $W_{co} = M \Lambda M^{-1}$.

$$\begin{aligned} \dot{z}(t) &= \tilde{A} z(t) + \tilde{B} u(t) \\ y(t) &= \tilde{C} z(t) \end{aligned} \tag{36}$$

$$\tilde{A} := M^{-1} A M, \;\; \tilde{B} := M^{-1} B, \;\; \tilde{C} := C M \tag{37}$$

The transformation M is chosen such that the controllability and observability gramians for the transformed system satisfy [18]

$$\tilde{W}_c = \tilde{W}_o = M^{-1} W_c M^{-1T} = M^T W_o M =: \Sigma \tag{38}$$

where Σ is a diagonal matrix that satisfies $\Sigma^2 = \Lambda$, and the diagonal elements of Σ, σ_i's, are known as the Hankel singular vales of the system, i.e.,

$$\Sigma = diag\{\alpha_1, \alpha_2, \cdots, \alpha_n\} \tag{39}$$

where σ_i are the Hankel singular values of the system G arranged in non-increasing order

$$\alpha_1 \geq \alpha_2 \geq \cdots \geq \alpha_n \geq 0 \tag{40}$$

In balanced truncation only states corresponding to large Hankel singular values are retained. Small Hankel singular values correspond to states which are deemed weakly controllable and weakly observable, and therefore deleted from the state-space model. For instance, if the first n_r states are retained then the resulting transformation is given by

$$M_r = P_r M \tag{41}$$

where P_r is the orthogonal projection of rank r.

The reduced order model is obtained by letting $x_r = P_r M x$ as follows

$$\begin{aligned} \dot{x}_r(t) &= A_r x_r(t) + B_r u(t) \\ y_r(t) &= C_r x_r(t) \end{aligned} \tag{42}$$

$$A_r := P_r M^{-1} A M P_r; \;\; B_r := P_r M^{-1} B, \;\; C_r := C M P_r$$

The error bound for the output is given by

$$\left\| y(t) - y_r(t) \right\|_2 \leq 2 \sum_{n_r+1}^{n} \sigma_i \left\| u(t) \right\|_2, \qquad \forall u \in L^2 \tag{43}$$

Balanced truncation is optimal in a precise sense when starting from the so-called Curtain-Glover balanced realization. To see this define a causal bounded input-output operator G acting on the standard space $L^2(-\infty, \infty)$ of absolutely square integrable functions defined on $(-\infty, \infty)$, into $L^2(-\infty, \infty)$ described by the convolution [18]

$$(Gu)(t) := \int_{-\infty}^{t} C e^{A(t-\tau)} B u(\tau) d\tau \tag{44}$$

Now, define the Hankel operator

$$\Gamma_G : L^2(-\infty, 0] \to L^2[0, \infty)$$

of G by

$$\Gamma_G := P_+ G \big|_{L^2(-\infty, 0]} \tag{45}$$

where $G\big|_{L^2(-\infty,0]}$ denotes the restriction of G to $L^2(-\infty,0]$, and P_+ is the orthogonal projection acting from $L^2(-\infty,\infty]$ into $L^2[0,\infty)$, i.e., P_+ is the truncation operator

$$P_+ f(t) = \begin{cases} f(t) & if \quad t \geq 0 \\ 0 & if \quad t < 0 \end{cases} \qquad f(t) \in L^2(-\infty,\infty) \tag{46}$$

Then, the Hankel operator Γ_G can be written as

$$\Gamma_G u(t) = \int_{-\infty}^{0} Ce^{A(t-\tau)}Bu(\tau)d\tau, \qquad for\ t \geq 0 \tag{47}$$

The Hankel operator Γ_G maps past inputs to future outputs. Expression (45) shows that the Hankel operator Γ_G is an integral operator mapping $L^2(-\infty,0)$ into $L^2[0,\infty)$, with kernel the impulse response $k(t,\tau)$ defined by

$$k(t,\tau) := Ce^{A(t-\tau)}B, \qquad \tau < 0, \qquad t \geq 0 \tag{48}$$

Balanced truncation is commonly thought to be a model reduction technique that is not optimal in any sense [22]. We show that this is not the case, and in fact balanced truncation is indeed optimal in the sense of the Hilbert-Schmidt. The techniques we use are reminiscent of the previous section and guarantee for the optimum to be a Hankel operator. This contrasts, for example, with the minimization in various norms addressed in [33] [34]. To see this note that the Hankel operator Γ_G has finite rank $k \leq n$ [18], and therefore belongs to the Hilbert-Schmidt class of operators acting from $L^2(-\infty,0]$ into $L^2[0,\infty)$. Let its spectral factorization be given by

$$\Gamma_G = \sum_{i=1}^{n} \sigma_i \chi_i \otimes \zeta_i, \quad \chi_i \in L^2(-\infty,0], \quad \zeta_i \in L^2[0,\infty) \tag{49}$$

where σ_i are the Hankel singular values of the system G ordered in decreasing order, i.e.,

$$\sigma_1 \geq \sigma_2 \geq \cdots \geq \sigma_{n-1} \geq \sigma_n \tag{50}$$

and $\{\chi_i\}_1^n$ and $\{\zeta_i\}_1^n$ are orthonormal sets in $L^2(-\infty,0]$ and $L^2[0,\infty)$, respectively. Next, consider the optimal distance minimization

$$\mu_{n_r} := \min_{n_r < k} \| \Gamma_G - \Gamma_{G_r} \|_{HS} \tag{51}$$

where Γ_{G_r} is an operator acting from $L^2(-\infty,0]$ into $L^2[0,\infty)$ of rank $n_r < n$. An application of identities (29) and (30) to the minimization (51) yields the *unique* optimum (since the distance minimization is posed in a Hilbert space)

$$\Gamma_{G_r} = \sum_{i=1}^{n_r} \sigma_i \chi_i \otimes \zeta_i \tag{52}$$

and the shortest distance

$$\mu_{n_r} = \| \sum_{i=1}^{n} \sigma_i \chi_i \otimes \zeta_i - \sum_{i=1}^{n_r} \sigma_i \chi_i \otimes \zeta_i \|_{HS} = \| \sum_{i=n_r+1}^{n} \sigma_i \chi_i \otimes \zeta_i \|_{HS} = (\sum_{i=n_r+1}^{n} \sigma_i^2)^{\frac{1}{2}} \tag{53}$$

The operator Γ_{G_r} is not necessarily a Hankel operator, however, we will show that starting from a specific balanced realization for the original system, the minimizing operator can be chosen to be a Hankel operator corresponding to the reduced order model. To do so let $\Gamma_G = U_G(\Gamma_G^* \Gamma_G)^{1/2}$ be a polar decomposition of Γ_G, applying (16) and (17) to Γ_G the vectors χ_i and ζ_i satisfy

$$\Gamma_G \chi_i = U_G (\Gamma_G^* \Gamma_G)^{\frac{1}{2}} \chi_i = \sigma_i \zeta_i, \quad i = 1, \cdots, n \tag{54}$$

$$\Gamma_G^* \chi_i = U_G^* (\Gamma_G \Gamma_G^*)^{\frac{1}{2}} \zeta_i = \sigma_i \chi_i, \quad i = 1, \cdots, n \tag{55}$$

That is, χ_i and ζ_i form a Schmidt pair for Γ_G. In terms of the Schmidt pair (49) implies that the Hankel operator Γ_G can be expressed as

$$(\Gamma_G u)(t) = \sum_{i=1}^{n} \zeta_i(t) \sigma_i \int_{-\infty}^{0} \chi_i(\tau) u(\tau) d\tau \tag{56}$$

We propose the following realization due to Curtain and Glover [34] for the impulse response $k(t, \tau)$ given in (48), for $i, j = 1, 2, \cdots, n$,

$$\begin{aligned} \tilde{A} &= (a_{ij}) := (\frac{\sigma_j}{\sigma_i})^{\frac{1}{2}} \int_{-\infty}^{0} \zeta_i^*(\tau) \dot{\zeta}_j(\tau) d\tau \\ \tilde{B} &:= (\sqrt{\sigma_1} \chi_1(0), \sqrt{\sigma_2} \chi_2(0), \cdots, \sqrt{\sigma_n} \chi_n(0))^T \\ \tilde{C} &:= (\sqrt{\sigma_1} \zeta_1(0), \sqrt{\sigma_2} \zeta_2(0), \cdots, \sqrt{\sigma_n} \zeta_n(0)) \end{aligned} \tag{57}$$

The corresponding semi-group can be computed as

$$e^{\tilde{A}t} = (\frac{\sigma_j}{\sigma_i})^{\frac{1}{2}} \int_{-\infty}^{0} \zeta_i^*(\tau) \zeta_j(t - \tau) d\tau \tag{58}$$

since

$$\lim_{t \to 0} \frac{1}{t} \int_{-\infty}^{0} \zeta_i^*(\tau) \zeta_j(\tau - t) d\tau = \int_{-\infty}^{0} \zeta_i^*(\tau) \dot{\zeta}_j(\tau) d\tau \tag{59}$$

Define the controllability and observability operators denoted Ψ_C and Ψ_O, respectively by [18]

$$\begin{aligned} &\Psi_C : L^2(-\infty, 0] \mapsto \mathbb{R}^n \\ &\Psi_C u := \int_0^{\infty} e^{\tilde{A}\tau} \tilde{B} u(\tau) d\tau \\ &\Psi_O : \mathbb{R}^n \mapsto L^2[0, \infty) \\ &\Psi_O x_0 : \tilde{C} e^{\tilde{A}t} x_0, \; t \geq 0 \end{aligned} \tag{60}$$

Note that [18]

$$\Gamma_G = \Psi_O \Psi_C \tag{61}$$

and using the realization (57), we have

$$(\Psi_O \Psi_C u)(t) = \sum_{i=1}^{n} \sigma_i \zeta_i \int_{-\infty}^{0} \chi_i^*(\tau) u(\tau) d\tau = (\Gamma_G u)(t) \tag{62}$$

and the observability gramian is given by

$$\Psi_O^* \Psi_O = \int_0^{\infty} e^{\tilde{A}^* t} \tilde{C}^* \tilde{C} e^{\tilde{A}t} dt \tag{63}$$

$$= (\int_0^{\infty} \sum_{i=1}^{n} \sum_{j=1}^{n} \sqrt{\sigma_i} \sqrt{\sigma_j} \zeta_i^*(t) \zeta_j(t) dt)$$

$$= (\sigma_i \delta_{ij}) = \Sigma = diag(\sigma_1, \sigma_2, \cdots, \sigma_n) \tag{64}$$

where δ_{ij} is the usual Kronecker delta.

Similarly the controllability gramian $\Psi_C \Psi_C^* = \Sigma$, and the realization $(\tilde{A}, \tilde{B}, \tilde{C})$ is therefore balanced. By the same token as POD using a similar expression as (27), define the Hankel operator corresponding to the n_r-th order model $\Gamma_{G_{n_r}}$ as

$$(\Gamma_{G_{n_r}} u)(t) = \sum_{i=1}^{n_r} \zeta_i(t) \sigma_i \int_{-\infty}^{0} \chi_i(\tau) u(\tau) d\tau \tag{65}$$

$$= \int_{-\infty}^{0} \tilde{C} P_r e^{\tilde{A}(t-\tau)} P_r \tilde{B} d\tau \tag{66}$$

$$= \int_{-\infty}^{0} \tilde{C} P_r (P_r e^{\tilde{A}(t-\tau)} P_r) P_r \tilde{B} d\tau \tag{67}$$

The last equality follows by (57), (58) and the fact that $P_r^2 = P_r$ (since P_r is a projection). Putting $\tilde{C}_r := \tilde{C} P_r$, $\tilde{B}_r := P_r \tilde{B}$ correspond to truncating $\tilde{C}$ and $\tilde{B}$, respectively, and (59) implies that $P_r e^{\tilde{A}(t-\tau)} P_r = e^{P_r \tilde{A} P_r (t-\tau)}$, and $\tilde{A}_r := P_r \tilde{A} P_r$ correspond to truncating the state space model $(\tilde{A}, \tilde{B}, \tilde{C})$ to n_r states, and the Hankel operator has rank n_r. Moreover,

$$\mu_{n_r} = \| \Gamma_G - \Gamma_{G_{n_r}} \|_{HS} = \left(\sum_{i=n_r+1}^{n} \sigma_i^2 \right)^{\frac{1}{2}} \tag{68}$$

By uniqueness of the minimizer in (51), expressions (65) and (68) imply that we must have $\Gamma_r \equiv \Gamma_{G_{n_r}}$.

In terms of kernel approximation, balanced truncation is a particular case of POD in the sense that the kernel we want to approximate is the impulse response of the system $k(t,\tau)$ defined in (51). The optimization index μ_{n_r} can then be written as in POD

$$\mu_{n_r}^2 = \min \{ \int_0^{\infty} \int_{-\infty}^{0} | k(t,\tau) - \sum_{i=1}^{n_r} f_i(t) g_i(\tau) |^2 \, d\tau dt : f_i \in L^2[0,\infty); g_i \in L^2(-\infty, 0] \} \tag{69}$$

$$= \int_0^{\infty} \int_{-\infty}^{0} | k(t,\tau) - \tilde{C}_r e^{\tilde{A}_r (t-\tau)} \tilde{B}_r |^2 \, d\tau dt \tag{70}$$

Expressions (54) and (70) show that balanced truncation is optimal in the sense of optimal approximation in the Hilbert-Schmidt norm of the Hankel operator Γ_G, and optimal in the sense of the $\|\bullet\|_2$-norm of kernels corresponding to impulse responses of linear time-invariant systems defined over $[0,\infty) \times (-\infty, 0]$. The linear time-invariant system framework allows the exact computations of the optimal lower order model approximation. This contrasts with POD which uses simulation data and particular open-loop inputs to generate snapshots.

IV. Prototype Problem: Nonlinear Convection

The specific problem geometry considered is shown in Figure 1. The idea and methods presented could be modified to apply to a different geometry or obstacle shape. A realistic example of this geometry in an aerodynamic application is a payload hatch open during flight with actuator

control only on the boundary. Let Ω_{gap} be the region defined by [a_1, a_2] x [b_1, b_2]. Let Ω_{full} be the region defined by (a_0, a_{end}) x (b_0, b_{end}). Then the problem domain is given by $\Omega = \Omega_{full} / \Omega_{gap}$. In this problem setup, Ω_{gap} is an obstacle. The system dynamics that act within the problem domain are described by the two dimensional (2D) Burger's equation

$$\frac{\partial}{\partial t} w(t,x,y) + \nabla \bullet F(w) = \frac{1}{r}\left(\frac{\partial^2}{\partial x^2} w(t,x,y) + \frac{\partial^2}{\partial y^2} w(t,x,y) \right) \tag{71}$$

where the form of $F(w)$ is

$$F(w) = \left[c_1 \frac{w^2(t,x,y)}{2} \qquad c_2 \frac{w^2(t,x,y)}{2} \right]^T \tag{72}$$

The value r is similar to the Reynolds number used in the Navier-Stokes Equation. This parameter controls how much nonlinearity is present in the problem. The 2D Burgers' equation is chosen as a surrogate for the Navier-Stokes equations, since it has a similar convective nonlinearity but can be coded on a PC.

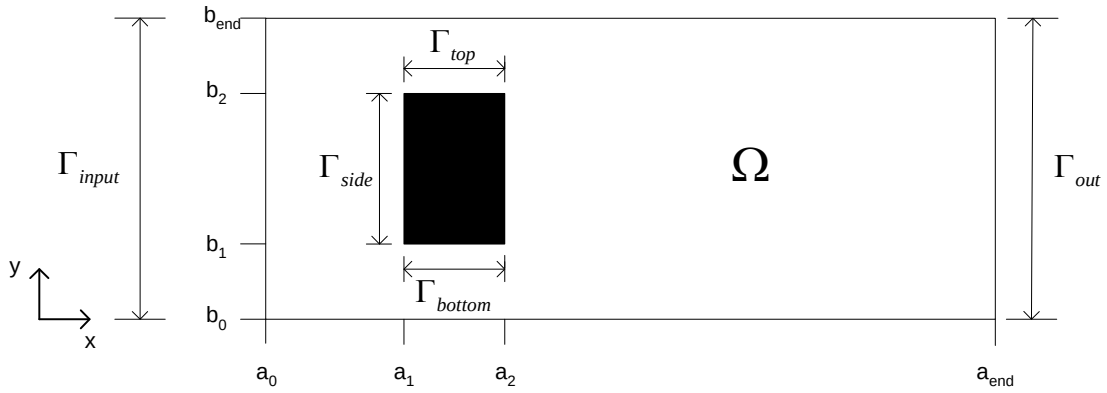

Figure 1. Problem Geometry

The boundary conditions on the top and bottom are described by the following equations

$$w(t,\Gamma_{bottom}) = u_{bottom}(t)\Psi_{bottom}(x) \tag{73}$$

$$w(t,\Gamma_{top}) = u_{top}(t)\Psi_{top}(x) \tag{74}$$

Here $u_{top}(t)$ and $u_{bottom}(t)$ are the control inputs on the top and bottom boundaries respectively, the spatial functions $\Psi_{top}(x)$ and $\Psi_{bottom}(x)$ describe the spatial effect that the controls have on the top and bottom boundaries. The boundary condition on the airflow intake side is $w(t,\Gamma_{in}) = f(y)$ and is parabolic in nature. The airflow outtake side has a Neumann boundary condition that has the form $\frac{\partial}{\partial x} w(t,\Gamma_{out}) = 0$. On all of the remaining boundaries of Ω, $w(t,x,y)$ is set equal to 0 for all values of t. Finally, the initial conditions for the interior are given by $w(0,x,y) = w_0(x,y) \in L^2(\Omega)$.

A numerical solution was found by simulation using a uniformly spaced grid. The resulting system model contains a little more than 2000 states. After this a method of optimal (with respect to average kinetic energy [27]) subspace detection was performed. POD is a method for model reduction that works on the idea that a set of basis vectors in an infinite dimensional space can be created that gives the best representation of typical system behavior for a fixed basis dimension size [27]. The method used for determining how many modes need to be retained is a design choice. A reasonable choice and the one used in this POD model construction were to look at the total energy captured. When a vector having significant system "energy" was found, it was forced to be perpendicular to all previously found $\varphi_k's$. A condition that 99.9% of system energy must be captured was used for determining how many system modes were needed. This condition was met by a 40 POD basis. Although this is a major reduction from the numeric solution, it will be shown that important system dynamics can be retained with even lower state number system models.

Other names for this decomposition are the Karhunen-Loéve decomposition [36][37], and principal component analysis [37]. Some applications have been in fluid mechanics, random variables, image processing, and data compression [10]. This decomposition method has been used extensively ([1] [4][8][7][11][12][13][14] [15][38][39][40][41]) to analyze experimental or simulation data and to extract the most dominant trends. The general approach of this method is to construct a series of solution "snapshots." These snapshots are solved by numeric simulations of the governing system equation(s) with a variety of input equations. The method of finding these solution snapshots is described in detail in [42][43]. The greatest strength of this method is that it provides a relevant and optimal set of basis functions that allows a low-dimensional subspace to be identified. This subspace allows us to derive a model when the governing equations are projected onto the subspace [27]. The snapshots are needed to generate the correlation matrix that can be used to find the POD basis. It is important to choose relevant input signals for the numerically simulated system. Further, these inputs should be similar to the expected inputs of the real system. In this way, the POD model should accurately represent the system in the normal operating range. In this paper the inputs used for system identification are of the form [12]

$$u_{bottom}(t) = \beta \sin(0.25t^2) \qquad u_{top}(t) = 0, \tag{75}$$

$$u_{bottom}(t) = 0 \qquad u_{top}(t) = \beta \sin(0.25t^2), \tag{76}$$

$$u_{bottom}(t) = \beta \sin(0.25t^2) \qquad u_{top}(t) = \beta \sin(0.25t^2)\ , \tag{77}$$

where the values for β are –3, -2, and –1 and the range for t is 0 to 10 seconds with a sample every 50 milliseconds. The squelch signal for all three values of β is shown in Figure 2.
The numerical simulation was performed to create the ensemble of solution snapshots $\{S_k(x,y)\}_{k=1}^{M}$ [12]. The snapshots refer to a collection of samples at specific points of individual solutions to the governing equation [27].

Each snapshot captures samples at specific points of the problem geometry while the control inputs are varied. The value for M (the number of snapshots) must be greater than the number of

modes that one will choose for the approximated system model. For a good representation M should be much larger than the desired size for the POD basis [12].

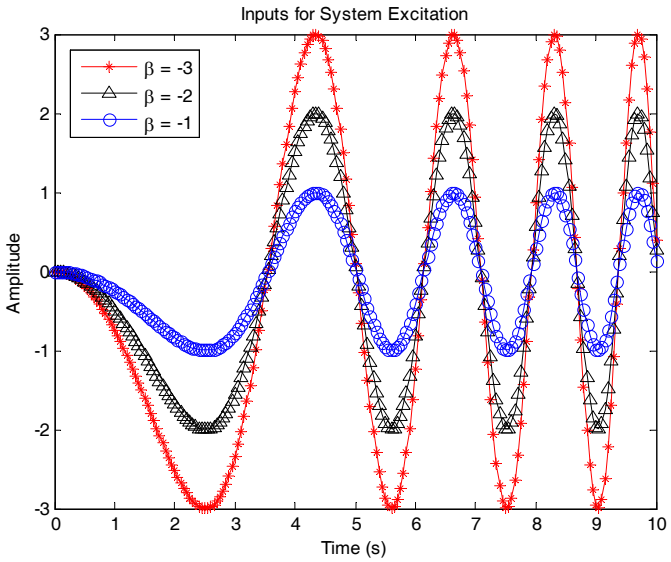

Figure 2. Test Inputs Used to Generate for Snapshots

The solution to the PDE is assumed to be finite energy, i.e., belongs to the Hilbert space $L^2([0,T)\times\Omega)$. The solution is approximated as

$$w(t,x,y)\approx\sum_{k=1}^{n}\alpha_k(t)\phi_k(x,y)\ \text{ where }\ \alpha_k\in L^2([0,T)),\ \phi_k(x,y)\in L^2(\Omega) \tag{78}$$

where $\alpha_k(t)\in L^2([0,T))$ are time varying coefficients that multiply the spatial functions $\phi_k(x,y)\in L^2(\Omega)$, where $L^2([0,T))$ and $L^2(\Omega)$ are the standard Hilbert spaces of absolutely square integrable functions defined, respectively, on the time interval $[0,T)$ and spatial domain Ω. The approximation (78) can be as accurate as desired since the tensor space

$$L^2([0,T))\otimes L^2(\Omega):=\left\{\sum_{k=1}^{n}\alpha_k(t)\phi_k(x,y),\ \alpha_k(t)\in L^2([0,T)),\ \phi_k(x,y)\in L^2(\Omega),\forall n\text{ integer}\right\} \tag{79}$$

is dense in $L^2([0,T)\times\Omega)$. Any basis for $L^2(\Omega)$ can be used to construct the approximation of the solution $w(t,x,y)$. Here we use the POD basis $\{\phi_k\}$ since it was shown to be optimal in the following sense

$$\mu_n:=\inf_{\substack{\alpha_k\in L^2([0,T)),\\ \phi_k(x,y)\in L^2(\Omega)}}\left\|w(t,x,y)-\sum_{k=1}^{n}\alpha_k(t)\phi_k(x,y)\right\|_2 \quad\text{and}\quad \mu_n\xrightarrow[n\to\infty]{}0 \tag{80}$$

where $\|\bullet\|_2$ is the norm of $L^2([0,T)\times\Omega)$. In section II it was shown that (80) corresponds to optimal approximation of an integral operator with kernel $w(t,x,y)$ in the HS norm by finite rank HS operators. A numerical solution was found by simulation using a uniformly spaced grid. The resulting system model contains a little more than 2000 states. The POD model construction is based on the total energy captured. A condition that 99.9% of system energy

must be captured was used for determining how many system modes were retained. Although this is a good reduction from the numerical solution, it is shown that important system dynamics can be retained with even lower order models. The general approach of POD is to construct a series of solution "snapshots." These snapshots were generated by numerical simulations of the 2D Burgers' equation with a variety of chirp input signals. Construction of a POD basis capable of spanning the baseline solution, as well as dynamics introduced by boundary actuation has been addressed using split POD. A Galerkin type projection using Divergence/Green's theorem results in a nonlinear Galerkin model. The Galerkin projection provides only a weak solution. However, this weak solution with finite difference approximations of the boundary conditions eventually leads to a nonlinear temporal model for the temporal or POD coefficients. This solution does not explicitly include the control inputs or boundary condition information into the governing equation. In order to do so an approximation of the partial derivatives is carried out including the control inputs and the boundary data. After substitutions $w(t,x,y)$ can be approximated as a linear combination of POD modes when the $\alpha_k(t)'s$ are solved in the nonlinear Galerkin model.

The ultimate goal for finding a solution to the governing equations is then to find the α_k's and φ_k's. The correlation matrix L, of size M x M, is composed of the inner products of the snapshots. Then in $L^2(\Omega)$

$$L_{k,j} = \langle S_k, S_j \rangle \tag{81}$$

$$\langle S_k, S_j \rangle = \int_\Omega S_k S_j^* dx\, dy \tag{82}$$

where * denotes complex conjugate transpose.

The term 'ensemble member' is used to describe one element of the collection of solution snapshots [12].

The function φ_i is chosen to maximize the average projection of the member u_i onto φ_i. This idea is expressed in the following manner [27][28]

$$\max_{\varphi \in L^2(\Omega)} \frac{\left|\langle u_i, \varphi_i \rangle\right|^2}{\left\|\varphi_i\right\|_2^2}. \tag{83}$$

A choice must be made on how many modes will be kept in the POD constructed subspace. This number can be chosen to be sufficiently large such that the majority of the system's total energy is captured. Additionally this number of modes to keep could be based upon the hardware abilities of the device doing the computations. The chosen number of modes to keep is denoted as n. A singular value decomposition of the matrix L is performed. The n largest eigenvalues $\{\lambda_1, \lambda_2, ..., \lambda_n\}$ of the matrix L are found and placed in descending order. Then the set of eigenvectors are identified to be $\{v_1, v_2, ...v_n\}$.

The resulting orthonormal POD basis of dimension *n* can be constructed using the information found from the correlation matrix *L*. First, the eigenvectors of *L* are weighted by their corresponding eigenvalues and normalized according to [12]

$$\lambda_k \left\| v_k \right\|^2 = 1 \text{, for k} = \{1, 2, ..., n\} . \tag{84}$$

Then, the POD basis set is formed according to

$$\varphi_k(x, y) = \sum_{j=1}^{M} v_{k,j} S_j(x, y), \tag{85}$$

with $v_{k,j}$ being the j^{th} component of the eigenvector v_k. Solving equation (85) gives the n φ_k's which constitute the POD basis of dimension *n*.

The governing equation is projected onto the POD basis. The projection is accomplished via a Galerkin type projection. The Galerkin projection results in only a weak solution to the PDE. However, this weak solution with finite difference approximations of the boundary conditions eventually leads to a nonlinear temporal model for the temporal or POD coefficients $\{\alpha_k\}$ [4]. Projecting (1) onto the POD basis yields [4]

$$\int_\Omega \frac{\partial}{\partial t} w(t, x, y) \varphi_k(x, y) dx = \frac{1}{\mathrm{Re}} \left(\int_{\partial\Omega} (\nabla w(t, x, y) \bullet n) \varphi_k(x, y) dA(x) - \int_\Omega \nabla w(t, x, y) \bullet \nabla \varphi_k(x, y) dx \right) -$$
$$\left(\int_{\partial\Omega} (F(w) \bullet n) \varphi_k(x, y) dA(x) - \int_\Omega F \bullet \nabla \varphi_k(x, y) dx \right)$$

where the first term on the right hand side is

$$\int_{\partial\Omega} (\nabla w(t, x, y) \bullet n) \varphi_k(x, y) dA(x) = \int_{a_1}^{a_2} \frac{\partial}{\partial y} w(t, x, b_1) \varphi_k(x, b_1) dx - \int_{a_1}^{a_2} \frac{\partial}{\partial y} w(t, x, b_2) \varphi_k(x, b_2)) dx \; -$$
$$\int_{b_0}^{b_{end}} \frac{\partial}{\partial x} w(t, a_0, y) \varphi_k(a_0, y) dy$$

The Neumann boundary condition forces the portion of the boundary integral over b_0 to b_{end} along a_{end} to be 0, i.e.,

$$\int_{b_0}^{b_{end}} \frac{\partial}{\partial x} w(t, a_{end}, y) \varphi_k(a_{end}, y) dy = 0 .$$

The second boundary integral is decomposed as follows

$$\int_{\partial\Omega} (F(w) \bullet n) \varphi_k(x, y) dA(x) = \frac{1}{2} \int_{b_0}^{b_{end}} (w(t, a_{end}, y)^2 \varphi_k(a_{end}, y) - f(y)^2 \varphi_k(a_0, y)) dy$$

This solution does not explicitly include the control inputs or boundary condition information into the governing equation. In order to do so an approximation of the partial derivatives is carried out including the control inputs and the boundary data. If *h* denotes the step size between the points on the uniform Cartesian grid used for the finite-difference solution, then we have [12]

$$\frac{\partial}{\partial y} w(t,x,b_1) \approx \frac{u_{bottom}(t)\Psi_{bottom}(x) - w(t,x,b_1 - h)}{h},$$

$$\frac{\partial}{\partial y} w(t,x,b_2) \approx \frac{w(t,x,b_2 + h) - u_{top}(t)\Psi_{top}(x)}{h}$$

$$\frac{\partial}{\partial x} w(t,a_0,y) \approx \frac{w(t,a_0 + h,y) - f(h)}{h}$$

After substitutions $w(t,x,y)$ can be approximated as a linear combination of POD modes when the α_k's are solved in the following system model. Then, the temporal model for the system is given by [12]

$$\dot{\alpha} = A\alpha + Bu + N(\alpha) + F, \qquad \alpha(0) = \alpha_o \tag{86}$$

where $\alpha \in \mathbb{R}^n$ and the matrices *A* is *n x n*, *B* is *n x 2*, *N* and *F* are both vectors n x 1.

The output equation will be simply chosen to be

$$y(t) = \alpha(t)$$

In this model the dimension of the state vector α is 40 which correspond to 40 POD modes. The first 8 POD modes corresponding to the first 8 temporal coefficients are shown in Figure 3. The first model corresponds to the baseline mode, and the remaining modes to actuated modes.

In Figure 4, dashed lines denote the linear combination of POD modes restricted to the boundary. Solid lines denote the boundary test inputs defined by

$$u_1(t) = \sin\left(\frac{3\pi t}{4}\right) \qquad u_2(t) = \sin\left(\frac{3\pi t}{2}\right)$$

As can be seen in Figure 4, there is very good agreement between the boundary conditions specified for the full order system and the linear combination of POD modes restricted to the boundary.

The goal of model reduction is to construct another nonlinear system [11][5]

$$\dot{\alpha}_r = A_r\alpha_r + B_r u + N_r(\alpha_r) + F_r \tag{87}$$

where $\alpha_r \in \mathbb{R}^r$ and $r < n$, such that the behavior of the two systems is similar for states in some region of the state space. The reduced model is derived via the construction of an immersion/projection pair

$$\alpha = \tilde{T}\alpha_r \qquad \alpha_r = T\alpha \qquad T\tilde{T} = I_r \tag{88}$$

where I_r is the $r \times r$ identity matrix, resulting in the following reduced model

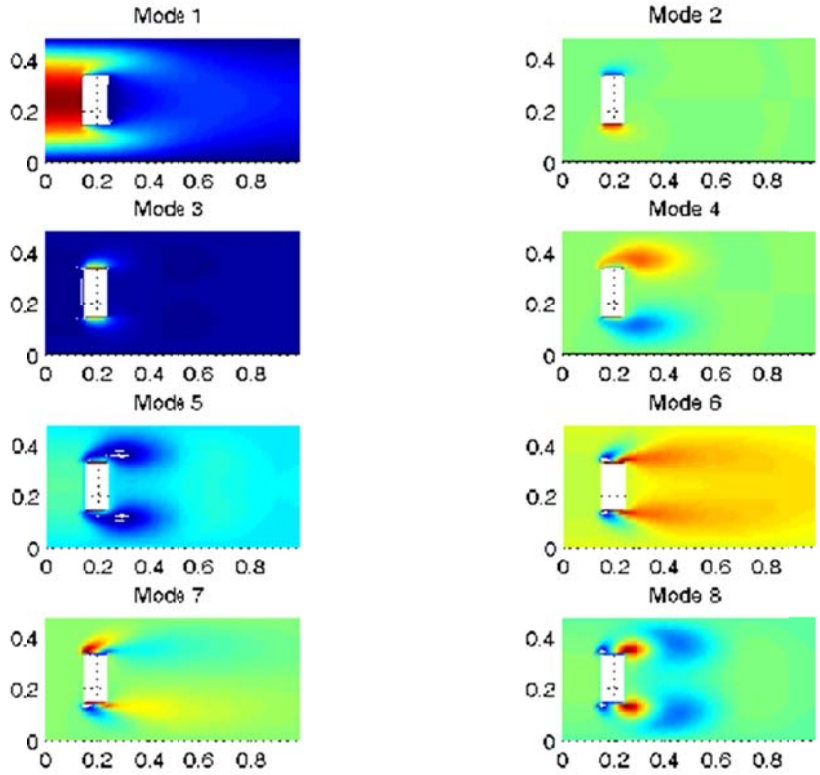

Figure 3: First Eight POD modes

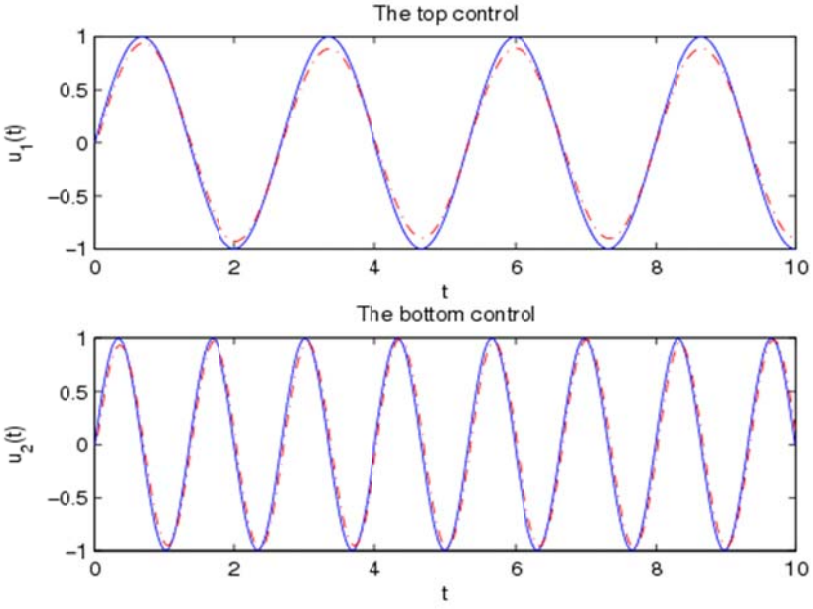

Figure 4: Boundary Control Accuracy

$$\begin{aligned} \dot{\alpha}_r &= TA\tilde{T}\alpha_r + TBu + TN(\tilde{T}\alpha_r) + TF \\ y(t) &= C\tilde{T}\alpha_r(t) \end{aligned} \tag{89}$$

This is carried out by developing an empirical balanced truncation algorithm which is based on experimental/simulation input-output measurements of the nonlinear Galerkin model. This is introduced in the next section.

V. A New Empirical Balanced Truncation

Balanced model reduction requires the knowledge of the controllability and observability gramians. The latter are obtained by solving Lyapunov equations, which is prohibitive for large scale systems. For a system with n states, the controllability and observability matrices are symmetric matrices and therefore solving each one of them involve finding n(n+1)/2 unknowns. An alternative is to develop a balanced truncation algorithm based on empirical gramians, which are constructed solely from a single simulation using a sufficiently rich input. The proposed empirical balanced truncation uses the Galerkin model with chirp signals as inputs to produce the outputs in the so-called Eigensystem Realization Algorithm (ERA). The latter estimates the system's Markov parameters that accurately reproduce the outputs. Balanced truncation is used to show that model reduction is still effective on ERA produced approximate systems. A new method of finding empirical controllability and observability gramians for the approximated system is introduced. After the empirical gramians are approximately balanced, the necessary transformation maps are applied back to the original system. The empirically balanced realization is then truncated to further reduce the system model size while retaining the most important system dynamics. The linear empirical balanced truncation algorithm is applied to the Galerkin model which is nonlinear. The rationale for doing so is that linear subspace approximations to exact submanifolds associated with nonlinear controllability and observability require only standard matrix manipulations utilizing simulation/experimental data.

The computation cost to solve large Lyapunov equations for the controllability and obervability gramians prompt us to propose a balanced truncation algorithm based on empirical gramians constructed from input-output data measurements. To this end, let us first introduce the *l*-step observability and *q*-step controllability matrices [47]

$$O_l := \begin{bmatrix} C \\ CA \\ CA^2 \\ \vdots \\ CA^{l-1} \end{bmatrix}, \quad R_q := \begin{bmatrix} B & AB & A^2B & \cdots & A^{q-1}B \end{bmatrix} \tag{90}$$

which give rise to the *l*-step observability and *q*-step controllability gramians

$$W_{ol} := O_l^* O_l, \qquad W_{cq} := R_q R_q^* \tag{91}$$

As the numbers *q* and *l* approach infinity, these empirical gramians approach the true gramians

$$\lim_{l\to\infty} W_{ol} = W_o, \qquad \lim_{q\to\infty} W_{cq} = W_c \tag{92}$$

The goal is to find a balancing transformation matrix M that will approximately balance the empirical gramians, i.e.,

$$\hat{W}_{cq} := MW_{cq}M^* = (M^*)^{-1}W_{ol}M^{-1} =: \hat{W}_{ol} = \Sigma \tag{93}$$

The matrix M can then be applied back to the original system model to produce an approximately balanced realization.

The product of the l-step controllability and the q-step observability matrices gives a Hankel[1] matrix, denoted H_{lq}, containing the Markov parameters $CA^kB,\ k = 0,1,\cdots$, of the system in the following way

$$H_{lq} := O_l R_q = \begin{bmatrix} CB & CAB & \cdots & CA^{q-1}B \\ CAB & CA^2B & \cdots & CA^qB \\ \vdots & \vdots & \ddots & \vdots \\ CA^{l-1}B & CA^lB & \cdots & CA^{l+q-2}B \end{bmatrix} \tag{94}$$

for integers l and q chosen such that [47]

$$rank(H_{lq}) = rank(H_{(l+1)(q+j)}) = n, \qquad \forall j \geq 1 \tag{95}$$

In terms of the SVD decomposition of H_{lq}

$$H_{lq} = U\Sigma V^* = [U_1 \ \ U_2]\begin{bmatrix} \Sigma_1 & 0 \\ 0 & 0 \end{bmatrix}\begin{bmatrix} V_1^* \\ V_2^* \end{bmatrix} \tag{96}$$

The balancing transformation M is constructed as

$$M = R_q V_1 \Sigma_1^{-1/2} \tag{97}$$

A straightforward computation shows

$$\hat{W}_{cq} := M^{-1}W_{cq}M^{*-1} = M^*W_{ol}M =: \hat{W}_{ol} = \Sigma_1 \tag{98}$$

Balanced truncation can be realized the usual way, if $\sigma_r \gg \sigma_{r+1}$ for some r then we can partition Σ_1 as

$$\Sigma_1 = \begin{bmatrix} \Sigma_r & 0 \\ 0 & \Sigma_{r+1} \end{bmatrix} \tag{99}$$

where

[1] A Hankel matrix is simply a matrix that has the i^{th} column identical to the i^{th} row.

$$\Sigma_r = diag(\sigma_1, \sigma_2, \cdots, \sigma_r), \quad \Sigma_{r+1} = diag(\sigma_{r+1}, \sigma_{r+2}, \cdots, \sigma_n) \tag{100}$$

A columwise conformal partition of U_1 and V_1

$$U_1 = [U_r \quad U_{n-r}], \quad V_1 = [V_r \quad V_{n-r}] \tag{101}$$

yields the immersion/projection pair

$$\tilde{T}_r = R_q V_r \Sigma_r^{-1/2}, \qquad T_r = \Sigma_r^{-1/2} U_r^* O_l, \qquad T_r \tilde{T}_r = I_r \tag{102}$$

and from which a reduced order r-dimensional model with state matrices is deduced

$$A_r = T_r A \tilde{T}_r \qquad B_r = T_r B \qquad C_r = C \tilde{T}_r \tag{103}$$

The above construction only requires estimates of the Markov parameters

$$CA^k B, \quad k = 0, 1, \cdots, l+q-1 \tag{104}$$

A basic relationship between the Markov parameters and the input and output relationship in discrete-time is

$$y(k) = \sum_{\ell=0}^{\infty} Y(\ell)\, u(k-\ell) \tag{105}$$

$$Y(0) = D, \; Y(1) = CB, \; Y(2) = CAB, \; \cdots, \; Y(k) = CA^{k-1}B \tag{106}$$

The Markov parameters can be computed from a single simulation/experiment in which a sufficiently rich input signal is applied and the output responses are collected. In the next section, the Discrete Fourier Transform (DFT) is used to map time domain data into spectral densities from which frequency response estimates are calculated using the Eigensystem Realization Algorithm (ERA) [44].

VI. Eigensystem Realization Algorithm (ERA)

Several frequency domain identification techniques are used in practice to identify the model parameters. One such method that is a well-defined frequency domain system identification is the Eigensystem Realization Algorithm (ERA) technique [44]. The ERA based system realization model is created directly from empirical data and frequency domain characteristics of transfer functions. This method is applied to discrete time versions of system models.

The ERA and the empirical balancing method have been in many cases [48][49][50][5] to identify the system based upon experimental or simulated results. The workhorse of the method involves finding the system Markov parameters to populate a matrix that gives the impulse response from each input to each output at various time steps.

The ERA process starts by forming the pulse response matrices *Y(k)*. Theoretically, pulse inputs are sufficient to excite the system to find the approximate frequency domain transfer function. The impulses must be timed so that they do not all occur at the same time so the individual impulses can overlap and are distinct for each input channel. However, practically a single impulse does not have enough energy to fully excite every state [50]. Each additional pulse response matrix is calculated such that $Y_{i,j}(k)$ is the i^{th} output at sample *k* resulting from a pulse input on the j^{th} input channel. The dimension of each of the Markov parameter matrices is *p x m* where *p* is the number of system inputs and *m* is the number of system outputs. As *k* increases,

the size of the Hankel matrix composed of the Markov parameters increases. This matrix does not have to be square. In practice, a broadband random input or a chirp is applied and estimates of the input autocorrelation and input/output cross-correlation are used to identify the system Markov parameters [44].

An alternative form to (105) can be created not using the actual outputs and inputs but replacing the output term by the cross-correlation between the inputs and the corresponding outputs [44]

$$R_{yu}(k) = \sum_{\ell=0}^{\infty} Y(\ell) R_{uu}(k-\ell) \tag{107}$$

where the length of the data sequence is m,

$$R_{uu}(k) = \frac{1}{m}\sum_{\tau=0}^{m-1} u(\tau)u^T(k-\tau) \quad \text{and} \quad R_{yu}(k) = \frac{1}{m}\sum_{\tau=0}^{m-1} y(\tau)u^T(k-\tau). \tag{108}$$

The basic process for finding the Markov parameters starts using the ratio of the power spectral density of the cross-correlation between the inputs and outputs and the power spectral density of the autocorrelation between the input signals.

These power spectral densities are given by the following

$$P_{yu}(k) = \frac{1}{m}\sum_{\tau=0}^{m-1} R_{yu}(\tau)e^{-j\frac{2\pi k}{m}\tau} \quad \text{and} \quad P_{uu}(k) = \frac{1}{m}\sum_{\tau=0}^{m-1} R_{uu}(\tau)e^{-j\frac{2\pi k}{m}\tau} \tag{109}$$

The ratio of the two power spectral densities is the frequency response function and is given by [44]

$$G(z_k) = \frac{P_{yu}(k)}{P_{uu}(k)}. \tag{110}$$

Then, the final step is to take the inverse Fourier transform to find the pulse response (Markov parameter) matrices [44]

$$Y_k := Y(k) = \sum_{\ell=0}^{\infty} G(z_k) e^{j\left(\frac{2\pi\ell}{m}\right)k}. \tag{111}$$

This system identification method can give good results even in the case where very noisy data is acquired. This ability lies in taking many more Markov parameters than the true system order. The computed Markov parameters that do not agree with the other data can effectively be filtered out of the frequency response function. The Hankel matrix containing the Markov parameters is of the following form [67]

$$H_{lq} = \begin{bmatrix} Y_1 & Y_2 & \cdots & Y_q \\ Y_2 & Y_3 & \cdots & Y_{q+1} \\ \vdots & \vdots & \vdots & \vdots \\ Y_l & Y_{l+1} & \cdots & Y_{q+l-1} \end{bmatrix} \tag{112}$$

The individual Y_k's correspond to the following sequence:

$$Y_0 = D,\ Y_1 = CB,\ Y_2 = CAB,\ \ldots,\ Y_k = CA^{k-1}B \tag{113}$$

In some cases the input data for the ERA method might be provided by an experiment on a real system. However, in this project a unique approach of using the Galerkin model in the place of the real system was used to generate the empirical data. The full order system model was created using finite-difference methods. Recall that the control inputs were explicitly placed in the boundary conditions because the control inputs do not show up explicitly in the two-dimensional burger's equation. However, the weak Galerkin model results in a nonlinear state space model that simplifies the relationship between the input and outputs.

The chirp signals used for the excitation of the Galerkin model are of the following form and are shown in Figure 5.

$$u_1(t) = -\sin(0.55t^2) \tag{114}$$

$$u_2(t) = -\sin(0.60t^2) \tag{115}$$

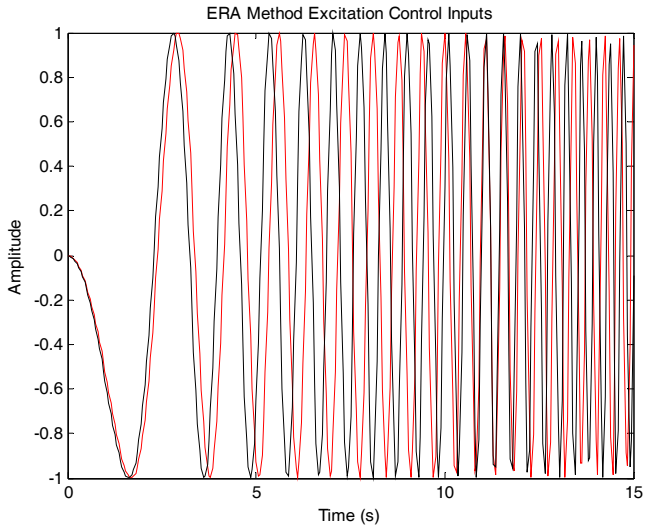

Figure 5. Excitation Inputs for ERA Method

VII. Application to the Galerkin Model

The empirical balanced truncation based on linear systems is applied to the Galerkin model

$$\dot{\alpha} = A\alpha + Bu + N(\alpha) + F, \qquad \alpha(0) = \alpha_o \tag{116}$$

which has an equilibrium in steady state, denoted by α_{ss}. The rationale for doing so is that linear subspace approximations to exact submanifolds associated with nonlinear controllability and observability require only standard matrix manipulations utilizing simulation/experimental data as explained in [49]. The computational advantages of the scheme presented here carry over directly to the nonlinear setting.

The reduced order model is derived as discussed through the construction of the immersion/projection nonlinear system pair

$$\alpha = \tilde{T}\alpha_r, \qquad \alpha_r = T\alpha \tag{117}$$

This results in the following reduced-order model

$$\dot{\alpha}_r = A_r\alpha_r + B_r u + N_r(\tilde{T}\alpha_r) + F_r, \qquad \alpha_r(0) = T\alpha_o \tag{118}$$

where

$$A_r := TA_r\tilde{T}, \qquad B_r := TB, \quad N_r := TN, \quad F_r := TF$$

If (116) has a linearization around the steady state equilibrium α_{ss}

$$\dot{\alpha} = A_\ell\alpha + B_\ell u, \qquad \alpha(0) = \alpha_o \tag{119}$$

where

$$A_\ell = \left.\frac{\partial(A\alpha + Bu(t) + N(\alpha) + F)}{\partial\alpha}\right|_{\alpha=\alpha_{ss}} \tag{120}$$

$$B_\ell = \left.\frac{\partial(A\alpha + Bu(t) + N(\alpha) + F)}{\partial u}\right|_{u} \tag{121}$$

and the reduced system linearization around the steady state equilibrium α_{ss}

$$\dot{\alpha}_r = A_{\ell r}\alpha_r + B_{\ell r}u, \qquad \alpha_r(0) = T\alpha_o \tag{122}$$

where

$$A_{\ell r} = \left.\frac{\partial(A_r\alpha_r + B_r u(t) + N_r(\tilde{T}\alpha_r) + F_r)}{\partial\alpha}\right|_{\alpha=\alpha_{ss}} \tag{123}$$

$$B_{\ell r} = \left.\frac{\partial(A_r\alpha_r + B_r u(t) + N_r(\tilde{T}\alpha_r) + F_r)}{\partial u}\right|_{u} \tag{124}$$

The linearization of both models about equilibrium α_{ss} are related by

$$A_{\ell r} = TA_\ell\tilde{T}, \qquad B_{\ell r} = TB_\ell$$

Empirical balanced truncation applied to the 40 order Galerkin model resulted in a 14^{th} order reduced model. The first 8 temporal coefficients of the 14 order reduced model and 2000 full order model are plotted in Figure 6. Figure 6 shows good agreement between the temporal coefficients.

In Figure 7, we compare the Hankel singular values of the 2000 full order linearized and reduced 14^{th} order empirical model. As expected the Hankel singular values corresponding to the

reduced order model are smaller than the full order model, nevertheless the Figure shows that they are close. In Figure 8 we compare the full order solution $w(t,x,y)$ of the Burgers' equation with the solution based on the 14^{th} order ERA model $w_r(t,x,y)$. The Figure shows that they behave similarly especially at the boundary where control is applied.

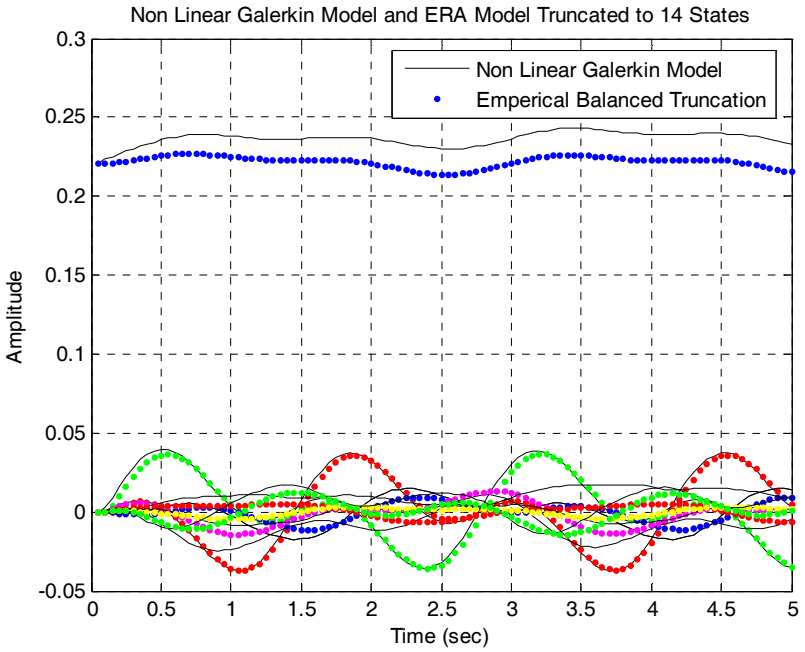

Figure 6. Projected and POD Model Coefficients.

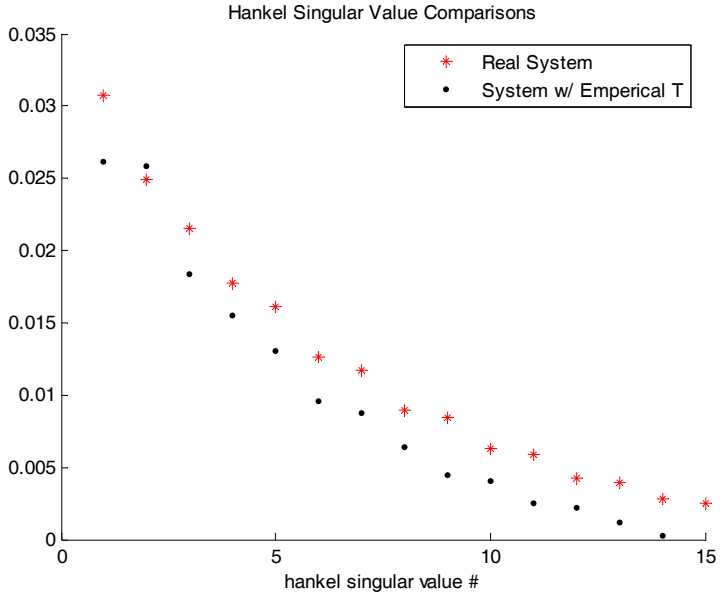

Figure 7. Comparison of Hankel Singular Values.

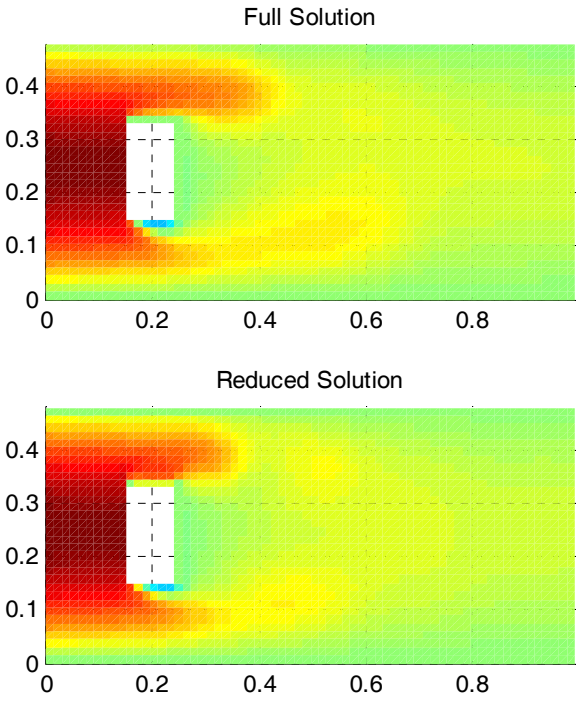

Figure 8. Full and Reduced Order Models' Responses.

VIII. A New Empirical Hankel Norm Model Reduction

In this section, we develop and apply an empirical Hankel norm model reduction technique to a Galerkin model. The latter is obtained by projecting the governing equations of a nonlinear convective flow on its proper orthogonal decomposition basis. The nonlinear convective flow is chosen as a prototype problem.

The proposed empirical Hankel norm model reduction uses the Galerkin model with a chirp signal as input to produce an approximate linear model and estimates its Markov parameters that accurately reproduce the output. A method of finding empirical controllability and observability gramians for the approximated system is discussed. After the empirical gramians are approximately balanced, the necessary balancing transformation matrix can be applied back to the original system to get an approximate balanced realization. Further, Hankel optimal norm reduction is applied to the latter model. Hankel model reduction uses the system operator induced norm instead of the average system energies used in POD and balanced model reduction techniques. The operator norm is a more precise and appropriate measure of system modeling errors. Application to the nonlinear convective flow as a prototype problem shows the effectiveness of the proposed empirical Hankel norm model reduction, and promise for application to the Navier-Stokes equations since the former has a similar nonlinearity.

Hankel norm approximation is an optimal model reduction in the sense of the operator norm of the Hankel operator associated to the system [51][18][19][52][53]. This makes it particularly useful for model reduction since it is desirable for the error induced norm between the original and reduced model be small. The idea is to approximate the Hankel operator associated to the system by another Hankel operator with lower rank in an optimal way. The error induced norm is the worst case error due to the input and making it small guarantees that the input-output behaviors of both the original and reduced models are close for any input. In practice the algorithm uses a balanced state space representation [18].

Hankel norm approximation provides a better error bound than balanced truncation and works well even when there is no Hankel singular value. However, there is no viable Hankel norm model reduction for nonlinear systems and we resort to constructing an approximate linear model from empirical data using the nonlinear Galerkin model.

Recall

$$(Gu)(t) \coloneqq \int_{-\infty}^{\infty} Ce^{A(t-\tau)}Bu(\tau)d\tau = y(t) \tag{125}$$

The Hankel operator Γ_G can be written as

$$\left(\Gamma_G u\right)(t) = \int_{-\infty}^{0} C\, e^{A(t-\tau)}\, B u(\tau)\, d\tau,\ t \geq 0 \tag{126}$$

The Hankel operator Γ_G maps past inputs to future outputs, and has finite rank *n*, that is, its range has finite dimension *n* if the state space has dimension *n* [18]. The Hankel singular values are the singular values of Γ_G.

The induced norm of Γ_G is defined by

$$\left\|\Gamma_G\right\| \coloneqq \sup_{\substack{u\in L^2(-\infty,0] \\ \|u\|_2 \leq 1}} \left\|\Gamma_G u\right\|_2 \tag{127}$$

Hankel model reduction is concerned with finding a reduced model G_r such that its associated Hankel operator Γ_{G_r} has rank, say $r < n$, in other words

$$\begin{aligned} \mu_r \coloneqq & \min_{r<n} \sup_{\substack{u\in L^2(-\infty,0] \\ \|u\|_2 \leq 1}} \left\|\Gamma_G u - \Gamma_{G_r} u\right\|_2 \\ = & \min_{r<n} \left\|\Gamma_G - \Gamma_{G_r}\right\| \end{aligned} \tag{128}$$

We need the balanced realization for (73). Partition the state matrices as [54]

$$\hat{A} = \begin{bmatrix} \overbrace{A_{11}}^{r\times r} & A_{12} \\ A_{21} & \underbrace{A_{22}}_{n-r\times n-r} \end{bmatrix}, \quad \hat{B} = \begin{bmatrix} B_1 \\ B_2 \end{bmatrix}, \quad \hat{C} = \begin{bmatrix} C_1 & C_2 \end{bmatrix} \tag{129}$$

and the balanced empirical gramians as

$$\Sigma_1 = \begin{bmatrix} \overbrace{\Sigma_{11}}^{r\times r} & 0 \\ 0 & \underbrace{\Sigma_{12}}_{n-r\times n-r} \end{bmatrix} \tag{130}$$

The Hankel reduced order model has then state space realization [54][18]

$$\begin{aligned} \dot{\tilde{x}}(t) &= A_r \tilde{x}(t) + B_r u(t) \\ \tilde{y}(t) &= C_r \tilde{x}(t) + D_r u(t) \end{aligned} \tag{131}$$

where

$$A_r = \Gamma^{-1}(\sigma_{r+1}{}^2 A_{11}^* + \Sigma_{12} A_{11} \Sigma_1 - \sigma_{r+1} C_1^* U B_1^*) \tag{132}$$

$$B_r = \Gamma^{-1}(\Sigma_{12} B_1 + \sigma_{r+1} C_1^* U) \tag{133}$$

$$C_r = C_1 \Sigma_{11} + \sigma_{r+1} U B_1^* \tag{134}$$

$$D_r = -\sigma_{r+1} U \tag{135}$$

And σ_{r+1} is the $r+1$ th Hankel singular value and U is a unitary matrix such that [18]

$$B_2 = -C_2^* U \tag{136}$$

$$\Gamma = \Sigma_{11}{}^2 - \sigma_{r+1}^2 I \tag{137}$$

The upper bound in terms of the induced norm is given by

$$\begin{aligned} \left\| G - G_r \right\| &:= \sup_{\substack{u \in L^2(-\infty,\infty) \\ \|u\|_2 \le 1}} \left\| Gu - G_r u \right\|_2 \\ &\le \left(\sigma_{r+1} + \sigma_{r+2} + \ldots + \sigma_n \right) \end{aligned} \tag{138}$$

In the next section, this procedure is applied to the nonlinear convective flow.

IX. Application to the Prototype Nonlinear Convective Flow

The empirical balanced truncation based on linear systems is applied to the Galerkin model

$$\dot{\alpha} = A\alpha + Bu + N(\alpha) + F, \quad \alpha(0) = \alpha_o \tag{139}$$

which has an equilibrium in steady state, denoted by α_{ss}.

The results obtained for the first eight temporal coefficients for the full order and the 8 order Hankel reduced model are shown in Figure 9. The Figure shows excellent agreement between them. In Figure 10, we compare the Hankel singular values of the full order linearized and Hankel reduced 8th order model. In Figure 11, the error between singular values of linearized full order and Hankel reduced models are plotted.

Note that from Figure 9 the reduced order Hankel model captures the largest singular values which matter most for the input-output behavior and control more accurately. The larger the order of the Hankel reduced model the smaller the error.

In Figure 12 we compare the full order solution of the Burgers' equation with the solution based on the 8th order Hankel reduced model. Figure 12 shows that they behave similarly especially at the boundary where control is applied.

In Figure 13, we compare the full order and reduced order solutions for both the empirical and Hankel models. The Figure shows that the lowest 8th order Hankel model retains the important behaviors of the flow.

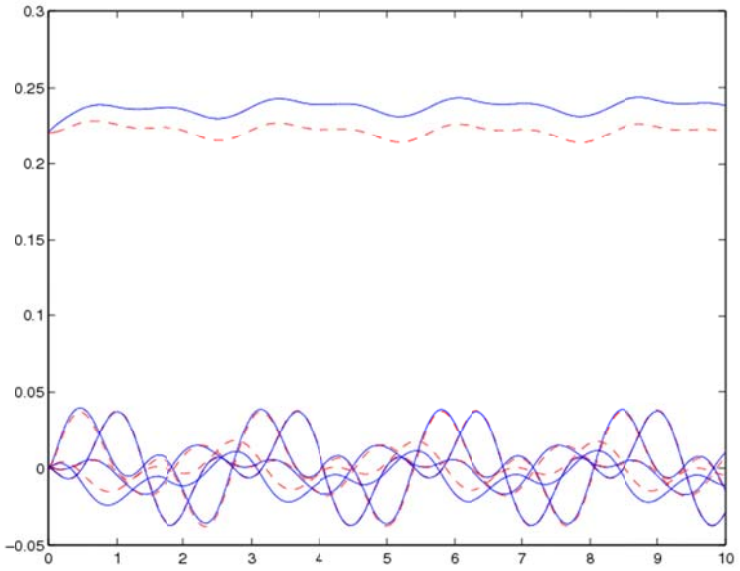

Figure 9. Projected and POD Model Coefficients.

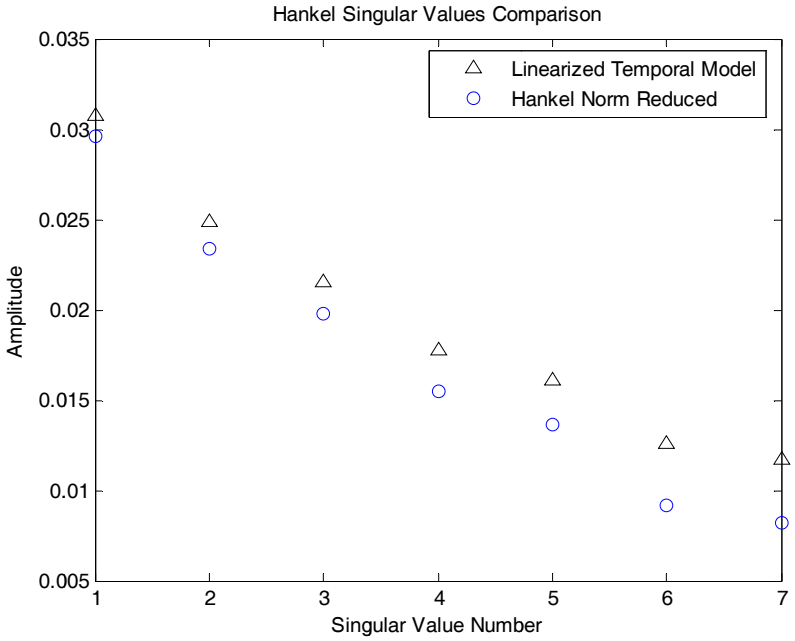

Figure 10. Comparison of Hankel Singular Values.

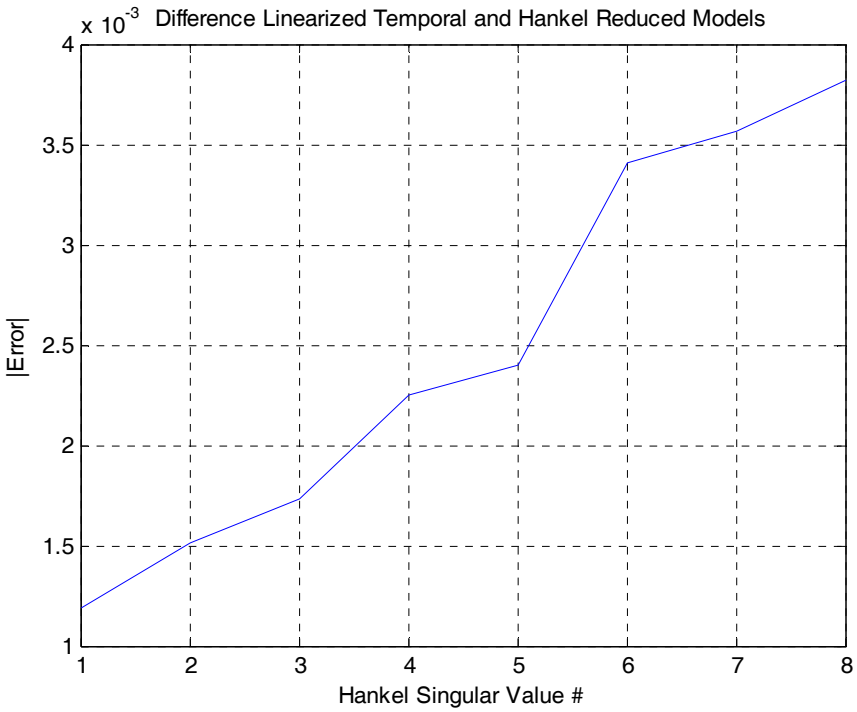

Figure 11. Error Between Singular values.

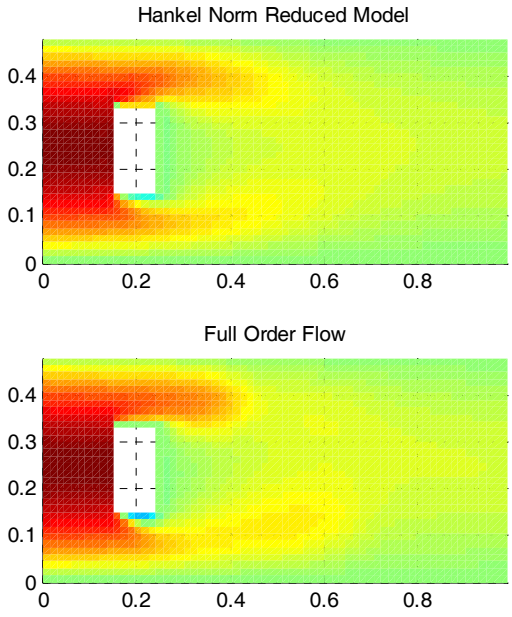

Figure 12. Full and Hankel Reduced Order Models Flow Responses

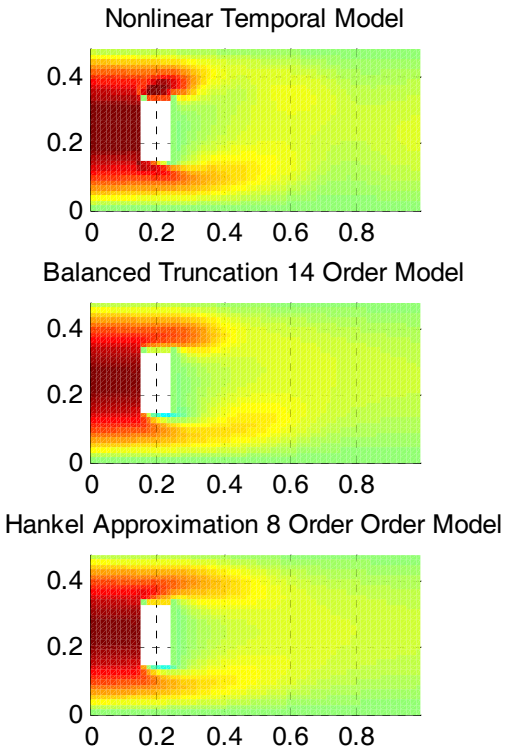

Figure 13. Full and Reduced Order Models' Responses.

X. H^{∞} Controller Design

In this section we consider the design of an H^{∞} controller using the Hankel reduced model. The motivation behind our choice is that H^{∞} controllers are robust against unmodeled or neglected dynamics, and unknown or unmeasurable disturbances [18][19]. A fixed reference signal $w_{ref}\ (x, y)$ is specified for the full order system. Projecting $w_{ref}\ (x, y)$ onto the POD basis yields tracking coefficients for the reduced order model, denoted by α_{ref} . The tracking problem is depicted in Figure 16, where *C* is the controller and *P* the plant represented by the dynamical equation (122). The computation of the H^{∞} is based on the 8^{th} order Hankel reduced model (131).

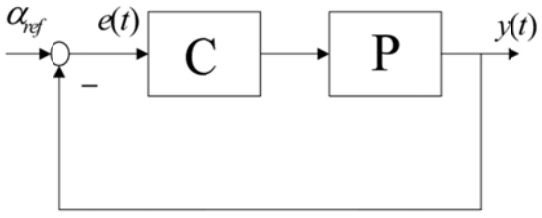

Figure 14. Closed-Loop Control System for Tracking

From Figure 14**,** for tracking purposes the controlled output is chosen to be the error signal *e* which is defined to be the difference between the reference α_{ref} and the actual output *y(t),* i.e.,

$$e(t) := \alpha(t) - \alpha_{ref} \tag{140}$$

The dynamics of the reduced model for tracking control represented in Figure 16 are then given by the state space equation

$$\begin{aligned} \dot{\tilde{x}}(t) &= A_r\tilde{x}(t) + \tilde{B}_1\alpha_{ref} + \tilde{B}_2u(t) \\ y(t) &= C_r\tilde{x}(t) + D_{11}\alpha_{ref} + D_{12}u(t) \\ e(t) &= -C_r\tilde{x}(t) + D_{21}\alpha_{ref}\, f + D_{22}u(t) \end{aligned} \tag{141}$$

The objective of the H^∞ controller *C* is to stabilize the closed-loop system and minimize the effect of α_{ref} on the error e by viewing α_{ref} as an unknown disturbance in L^2 of unit $\|\bullet\|_2$-norm. From Figure 14, in terms of transfer function matrices of *P* and *C*, the transfer matrix from α_{ref} to *e* is given by the sensitivity function $T_{e\alpha_{ref}}$ defined by

$$T_{e\alpha_{ref}} := (I + PC)^{-1}\alpha_{ref} \tag{142}$$

We compute the worst-case disturbance transmission error due to α_{ref}, i.e.,

$$\sup_{\|\alpha_{ref}\|_2 \le 1} \|e\|_2 \tag{143}$$

which is given by

$$\sup_{\|\alpha_{ref}\|_2 \le 1} \|e\|_2 = ess \sup_{0 \le \omega < \infty} \sigma\left(T_{e\alpha_{ref}}(j\omega)\right) =: \left\|T_{e\alpha_{ref}}\right\|_\infty \tag{144}$$

where ess sup denotes the essential supremum, and $\sigma(\bullet)$ the maximum singular value of its argument.

The H^∞ control design reduces to the following optimization: Find *C* such that the closed-loop system is robustly stable and

$$\mu := \min_C \left\|T_{e\alpha_{ref}}\right\|_\infty \tag{145}$$

The solution of (145) is textbook material. There are Riccati-based and linear matrix inequalities (LMIs) based techniques to solve (113) [18]. In this work, we use the LMI approach proposed in Matlab LMI toolbox because of its numerical robustness and stability.

After computing the H^{∞} controller we close the loop on the original full order model. The controller is only 8th order since based on the 8th order Hankel reduced model. The controlled closed-loop temporal coefficients $\{\alpha_k\}$ are plotted for the first 8 coefficients in Figure 15.

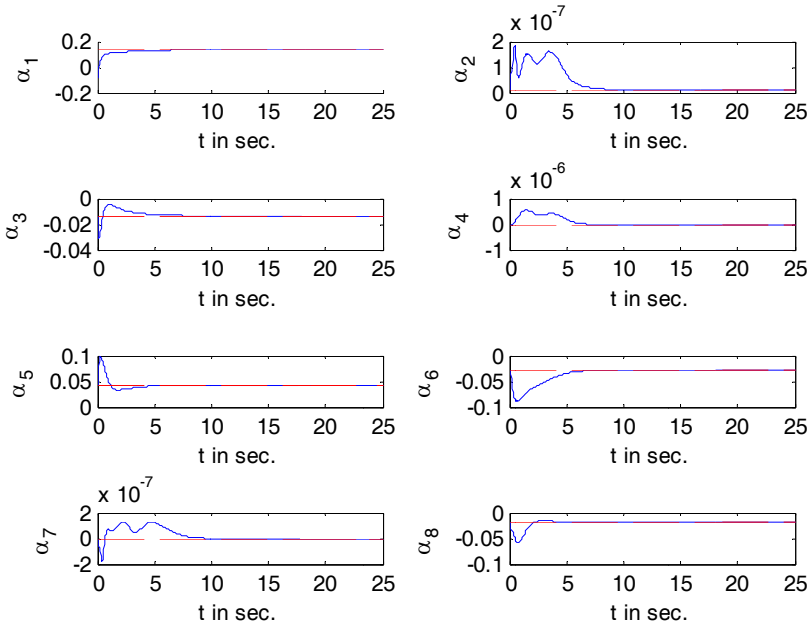

Figure 15. Full Order Closed-Loop System Tracking Response

The projected onto the POD basis initial condition and reference shown in Figure 16.

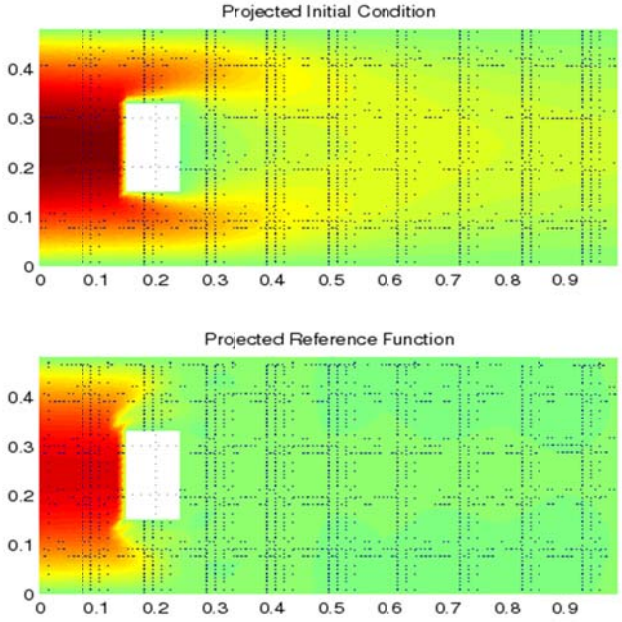

Figure 16. Flow Initial Condition and Reference

The controlled flow with the action of the boundary controller is shown in Figure 17, which shows that the flow tracks the reference.

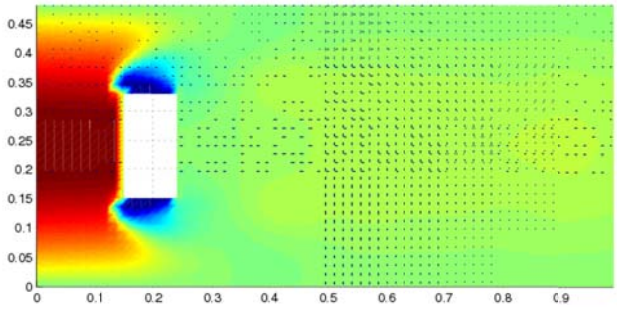

Figure 17. Controlled Flow

XI. Model Estimation for NACA 4412 POD Coefficients Based on Raw Pressure Surface Sensors Measurements

In this section, we consider a 2D flow control problem over the NACA 4412 airfoil [55][56][57]. The latter is a model constructed from PIV experimental measurements. The motivation for this problem is minimization of aero-optic distortion in a bluff-body flow. Here we are primarily concerned with model estimation of the temporal POD coefficients using raw experimental measurements provided by Glauser's flow control group at Syracuse University. The POD coefficients data are obtained from stochastic estimation based on 11 pressure sensors along the chord (surface measurements) as shown in Figure 18 [57].

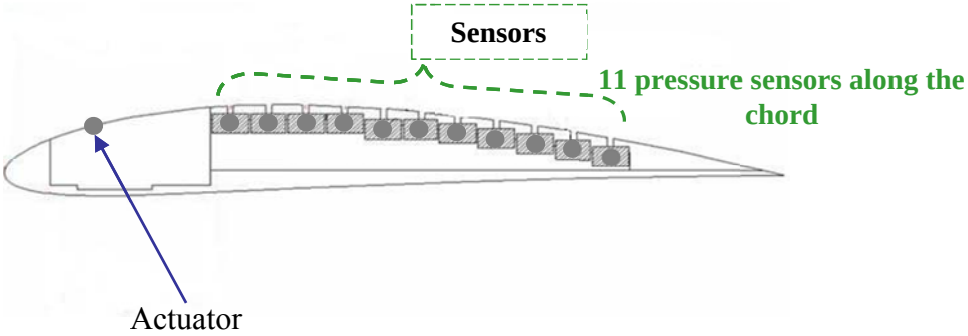

Figure 18. NACA 4412 Airfoil

The NACA 4412 experiment parameters are [57]

- The Flow speed: $U\infty = 10$ m.s^{-1}
- Airfoil chord: 20 cm
- Reynolds number: Re ~ 135,000
- Natural stall angle: $\alpha = 15°$

We describe the procedure employed to estimate the POD model parameters and states associated with the model using the EM algorithm [58] together with Kalman filtering [59]. We use the state space model

$$\begin{aligned} x_{t+1} &= A_t x_t + B_t w_t \\ y_t &= C_t x_t + D_t v_t \end{aligned} \tag{146}$$

where $x_t \in \Re^n$ is a state vector, $y_t \in \Re^d$ is a measurement vector, $w_t \in \Re^m$ is a state noise, and $v_t \in \Re^d$ is a measurement noise. The noise processes w_t and v_t are assumed to be independent zero mean and unit variance Gaussian processes. Further, the noises are independent of the initial state x_0, which is assumed to be Gaussian distributed.

The unknown system parameters $\theta_t = \{A_t, B_t, C_t, D_t\}$ as well as the system states x_t are estimated through the measurement data, $Y_N = \{y_1, y_2, ..., y_N\}$ obtained from surface pressure sensors. The methodology employed is recursive and based on the EM algorithm together with the Kalman filter. This is particularly useful for on-line implementation with the objective of real time control. The Kalman filter is discussed next.

A. Model State Estimation: The Kalman Filter

The Kalman filter estimates the channel states x_t for given system parameter $\theta = \{A, B, C, D\}$ and measurements Y_N. It is described by the following equations [59]

$$\begin{aligned} \hat{x}_{t|t} &= A\hat{x}_{t-1|t-1} + P_{t|t} C^T D^{-2} \left(y_t - CA\hat{x}_{t-1|t-1} \right) \\ \hat{x}_{t|t-1} &= A\hat{x}_{t-1|t-1} \\ \hat{x}_{0|0} &= m_0 \end{aligned} \tag{147}$$

where $t = 0, 1, 2, \cdots, N$, and $P_{t|t}$ is given by:

$$\begin{aligned} \overline{P}_{t|t}^{-1} &= P_{t-1|t-1}^{-1} + A^T B^{-2} A \\ P_{t|t}^{-1} &= C^T D^{-2} C + B^{-2} - B^{-2} \overline{P}_{t|t} A^T B^{-2} \\ P_{t|t-1} &= A P_{t-1|t-1} A^T + B^2 \end{aligned} \tag{148}$$

The channel parameters $\theta = \{A, B, C, D\}$ are estimated using the EM algorithm which is introduced next.

B. Model Parameter Estimation: The EM Algorithm

The EM algorithm uses a bank of Kalman filters to yield a maximum likelihood (ML) parameter estimate of the Gaussian state space model.

Let P_0 denote a fixed probability measure; and $\{P_\theta; \theta \in \Theta\}$ denotes a family of probability measures induced by the system parameters θ. If the original model is a white noise sequence, then $\{P_\theta; \theta \in \Theta\}$ is absolutely continuous with respect to P_0 [60]. Moreover, it can be shown that under P_0 we have:

$$P_0: \quad \begin{cases} x_{t+1} = w_t \\ y_t = v_t \end{cases} \tag{149}$$

The EM algorithm is an iterative scheme for computing the ML estimate of the system parameters θ, given the data Y_N. Specifically, each iteration of the EM algorithm consists of two steps: The expectation step and the maximization step.

The expectation step evaluates the conditional expectation of the log-likelihood function given the complete data, and is described by

$$\Lambda(\theta, \theta_l) = E_{\theta_l}\left\{ \log \frac{dP_\theta}{dP_{\theta_l}} \mid Y_N \right\} \tag{150}$$

where θ_l denotes the estimated system parameters at the *l*th iteration. The maximization step finds:

$$\theta_{l+1} \in \arg\max_{\theta \in \Theta} \ \Lambda(\theta, \theta_l) \tag{151}$$

The expectation and maximization steps are repeated until the sequence of model parameters converge by testing $\|\theta_l - \theta_{l+1}\|$ to be less than the required accuracy.

The EM algorithm is described by the following equations [58]

$$
\begin{aligned}
\hat{A} &= E\left(\sum_{t=1}^{N} x_t x_{t-1}^T \mid Y_N\right) \times \left[E\left(\sum_{t=1}^{N} x_t x_t^T \mid Y_N\right)\right]^{-1} \\
\hat{B}^2 &= \frac{1}{N} E\left(\sum_{t=1}^{N} \left((x_t - Ax_{t-1})(x_t - Ax_{t-1})^T\right) \mid Y_N\right) \\
&= \frac{1}{N} E\left(\sum_{t=1}^{N} \left(\left(x_t x_t^T\right) - A\left(x_t x_{t-1}^T\right)^T - \left(x_t x_{t-1}^T\right) A^T + A\left(x_{t-1} x_{t-1}^T\right) A^T\right) \mid Y_N\right) \\
\hat{C} &= E\left(\sum_{t=1}^{N} y_t x_t^T \mid Y_N\right) \times \left[E\left(\sum_{t=1}^{N} x_t x_t^T \mid Y_N\right)\right]^{-1} \\
\hat{D}^2 &= \frac{1}{N} E\left(\sum_{t=1}^{N} \left((y_t - Cx_t)(y_t - Cx_t)^T\right) \mid Y_N\right) \\
&= \frac{1}{N} E\left(\sum_{t=1}^{N} \left(\left(y_t y_t^T\right) - A\left(y_t x_t^T\right) C^T - C\left(y_t x_t^T\right)^T + C\left(x_t x_t^T\right) C^T\right) \mid Y_N\right)
\end{aligned}
\tag{152}
$$

where $B^2 = BB^T$, $D^2 = DD^T$, $E(\cdot)$ denotes the expectation operator. These system parameters $\left\{\hat{A}, \hat{B}^2, \hat{C}, \hat{D}^2\right\}$ can be computed from the following conditional expectations [58]

$$
\begin{aligned}
L_N^{(1)} &= E\left\{\sum_{t=1}^{N} x_t^T Q x_t \mid Y_N\right\} \\
L_N^{(2)} &= E\left\{\sum_{t=1}^{N} x_{t-1}^T Q x_{t-1} \mid Y_N\right\} \\
L_N^{(3)} &= E\left\{\sum_{t=1}^{N} \left[x_t^T R x_{t-1} + x_{t-1}^T R^T x_t\right] \mid Y_N\right\} \\
L_N^{(4)} &= E\left\{\sum_{t=1}^{N} \left[x_t^T S y_t + y_t^T S^T x_t\right] \mid Y_N\right\}
\end{aligned}
\tag{153}
$$

where *Q*, *R* and *S* are given by:

$$
\begin{aligned}
Q &= \left\{\frac{e_i e_j^T + e_j e_i^T}{2};\ i, j = 1, 2, \ldots n\right\} \\
R &= \left\{\frac{e_i e_j^T}{2};\ i, j = 1, 2, \ldots n\right\} \\
S &= \left\{\frac{e_i e_n^T}{2};\ i = 1, 2, \ldots m;\ n = 1, 2, .. d\right\}
\end{aligned}
\tag{154}
$$

in which e_i is the unit vector in the Euclidean space; that is $e_i = 1$ in the *i*th position, and *0* elsewhere. For instance, consider the case *n* = *m* = 2, then $E\left(\sum_{t=1}^{N} x_t x_{t-1}^T \mid Y_N\right)$ can be computed as:

$$E\left(\sum_{t=1}^{N} x_t x_{t-1}^T \mid Y_N\right)=\begin{bmatrix} L_N^{(3)}(R_{11}) & L_N^{(3)}(R_{12}) \\ L_N^{(3)}(R_{21}) & L_N^{(3)}(R_{22}) \end{bmatrix} \tag{155}$$

where $R_{ij}=\left\{\frac{e_i e_j^T}{2};\ i,j=1,2\right\}$. The other terms in (155) can be computed similarly.

The conditional expectations $\left\{L_N^{(1)}, L_N^{(2)}, L_N^{(3)}, L_N^{(4)}\right\}$ can be estimated from measurements Y_N as follows:

1) Filter estimate of $L_N^{(1)}$:

$$\begin{aligned} L_N^{(1)} &= E\left\{\sum_{t=1}^{N} x_t^T Q x_t \mid Y_N\right\} \\ &= -\frac{1}{2}Tr\left(N_N^{(1)} P_{N|N}\right)-\frac{1}{2}\sum_{t=1}^{N} Tr\left(N_{t-1}^{(1)}\overline{P}_{t|t}\right) \\ &\quad -\frac{1}{2}\sum_{t=1}^{N}\begin{pmatrix} -2x_{t|t}^T P_{t|t}^{-1} r_t^{(1)} + 2x_{t|t-1}^T P_{t|t-1}^{-1} r_{t|t-1}^{(1)} - x_{t|t}^T N_t^{(1)} x_{t|t} \\ + x_{t|t-1}^T B^{-2} A\overline{P}_{t|t} N_{t-1}^{(1)} \overline{P}_{t|t} A^T B^{-2} x_{t|t-1} \end{pmatrix} \end{aligned} \tag{156}$$

where $Tr(\cdot)$ denotes the matrix trace. In (115), $r_t^{(1)}$ and $N_t^{(1)}$ satisfy the following recursions:

$$\begin{cases} r_t^{(1)} = \left(A - P_{t|t} C^T D^{-2} CA\right) r_{t-1}^{(1)} + 2P_{t|t} Q x_{t|t-1} \\ \qquad\quad - P_{t|t} N_t^{(1)} P_{t|t} C^T D^{-2}\left(y_t - Cx_{t|t-1}\right) \\ r_{t|t-1}^{(1)} = A r_t^{(1)} \\ r_0^{(1)} = 0_{m\times 1} \end{cases}$$
$$\begin{cases} N_t^{(1)} = B^{-2} A\overline{P}_{t|t} N_{t-1}^{(1)} \overline{P}_{t|t} A^T B^{-2} - 2Q \\ N_0^{(1)} = 0_{m\times m} \end{cases} \tag{157}$$

2) Filter estimate of $L_N^{(2)}$:

$$\begin{aligned} L_N^{(2)} &= E\left\{\sum_{t=1}^{N} x_{t-1}^T Q x_{t-1} \mid Y_N\right\} \\ &= E_\theta\left\{x_0^T Q x_0 \mid Y_N\right\} + E_\theta\left\{\sum_{t=2}^{N} x_{t-1}^T Q x_{t-1} \mid Y_N\right\} \\ &= E_\theta\left\{x_0^T Q x_0 \mid Y_N\right\} + E_\theta\left\{\sum_{t=1}^{N} x_t^T Q x_t \mid Y_N\right\} - E_\theta\left\{x_N^T Q x_N \mid Y_N\right\} \end{aligned} \tag{158}$$

Therefore, $L_N^{(2)}$ can be obtained from $L_N^{(1)}$.

3) Filter estimate of $L_N^{(3)}$:

$$\begin{aligned} L_N^{(3)} &= E\left\{\sum_{t=1}^{N}\left(x_t^T R x_{t-1} + x_{t-1}^T R^T x_t\right) | Y_N\right\} \\ &= -\frac{1}{2}Tr\left(N_N^{(3)} P_{N|N}\right) - \frac{1}{2}\sum_{t=1}^{N} Tr\left(N_{t-1}^{(3)} \bar{P}_{t|t}\right) \\ &-\frac{1}{2}\sum_{t=1}^{N}\begin{pmatrix} -2x_{t|t}^T P_{t|t}^{-1} r_t^{(3)} + 2x_{t|t-1}^T P_{t|t-1}^{-1} r_{t|t-1}^{(3)} - x_{t|t}^T N_t^{(3)} x_{t|t} \\ +x_{t|t-1}^T B^{-2} A \bar{P}_{t|t} N_{t-1}^{(3)} \bar{P}_{t|t} A^T B^{-2} x_{t|t-1} \end{pmatrix} \end{aligned} \tag{159}$$

In this case, $r_t^{(3)}$ and $N_t^{(3)}$ satisfy the following recursions:

$$\begin{cases} r_t^{(3)} = \left(A - P_{t|t} C^T D^{-2} CA\right) r_{t-1}^{(3)} - P_{t|t} N_t^{(3)} P_{t|t} C^T D^{-2}\left(y_t - C x_{t|t-1}\right) \\ \quad + \left(2P_{t|t} R + 2P_{t|t} B^{-2} A \bar{P}_{t|t} R^T A\right) x_{t-1|t-1} \\ r_{t|t-1}^{(3)} = A r_t^{(3)} \\ r_0^{(3)} = 0_{m\times 1} \end{cases} \tag{160}$$

$$\begin{cases} N_t^{(3)} = B^{-2} A \bar{P}_{t|t} N_{t-1}^{(3)} \bar{P}_{t|t} A^T B^{-2} - 2R\bar{P}_{t|t} A^T B^{-2} \\ \quad - 2B^{-2} A \bar{P}_{t|t} R^T \\ N_0^{(3)} = 0_{m\times m} \end{cases}$$

4) Filter estimate of $L_N^{(4)}$:

$$\begin{aligned} L_N^{(4)} &= E\left\{\sum_{t=1}^{N}\left(x_t^T S y_t + y_t^T S^T x_t\right) | Y_N\right\} \\ &= \sum_{t=1}^{N}\left(x_{t|t}^T P_{t|t}^{-1} r_t^{(4)} - x_{t|t-1}^T P_{t|t-1}^{-1} r_{t|t-1}^{(4)}\right) \end{aligned} \tag{161}$$

where $r_t^{(4)}$ satisfy the following recursions:

$$\begin{cases} r_t^{(4)} = (A - P_{t|t} C^T D^{-2} CA) r_{t-1}^{(4)} + 2P_{t|t} S y_t \\ r_{t|t-1}^{(4)} = A r_t^{(4)} \\ r_0^{(4)} = 0_{m\times 1} \end{cases} \tag{162}$$

Using the filters for $L_N^{(i)}$ $(i = 1,2,3,4)$ and the Kalman filter described earlier, the system parameters $\theta_t = \{A_t, B_t, C_t, D_t\}$ are estimated through the EM algorithm described in (155). Numerical results that show the applicability of the above algorithm in estimating the POD coefficients model parameters as well as the model states are showed below.

The proposed estimation algorithm was used in conjunction with 1200 samples of raw data (non-filtered) which are used to estimate recursively the model. Figure 19 and Figure 20 show the two first POD coefficients. It can be seen that there is excellent agreement with the outputs of the proposed model and raw data. That is, once the model is in place; the raw measurement data can be generated using the proposed model. In Figure 21 we zoom in on the 2nd mode.

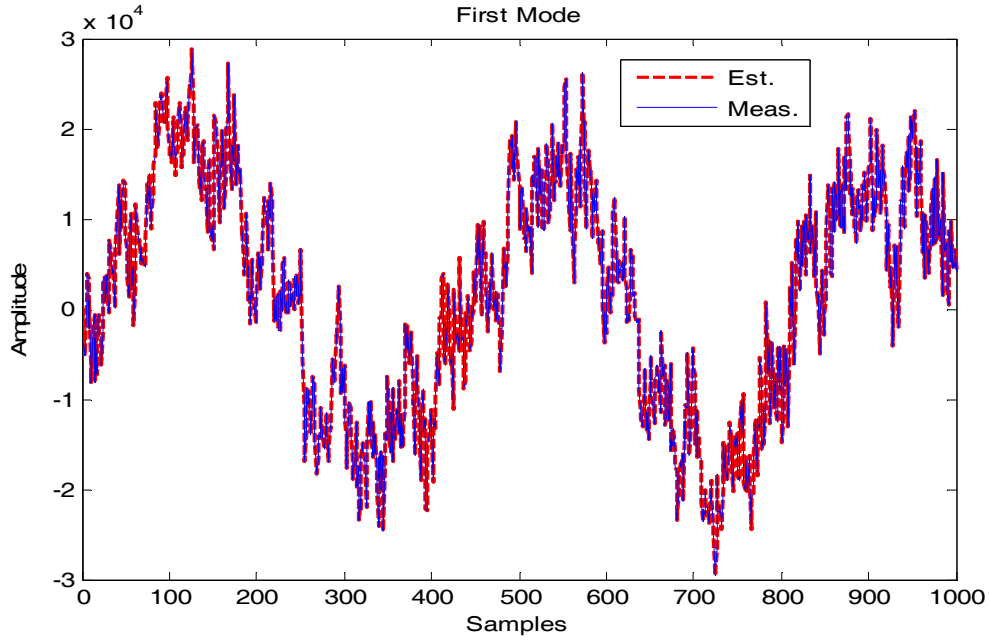

Figure 19. First Mode Coefficient

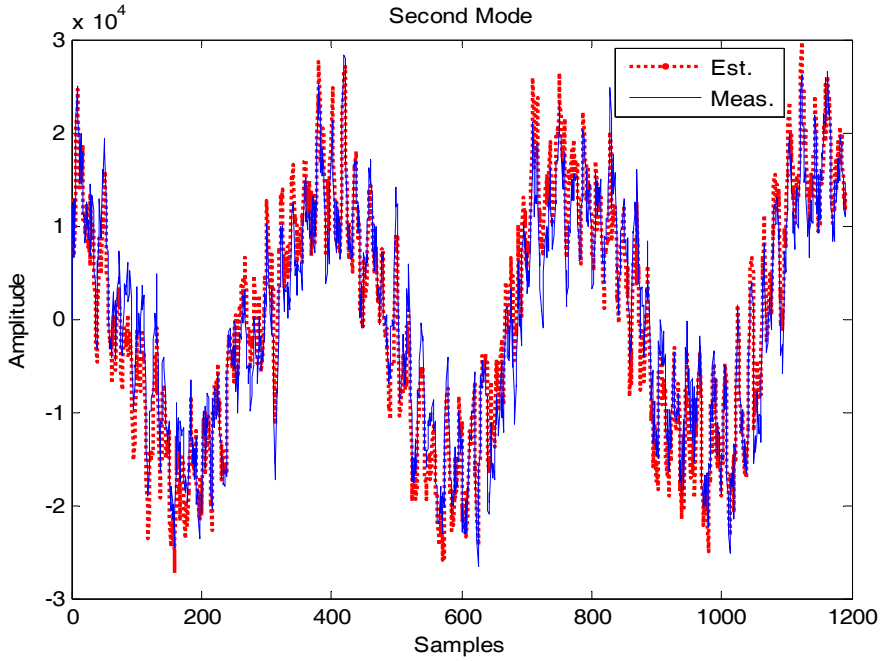

Figure 20. Second Mode Coefficient

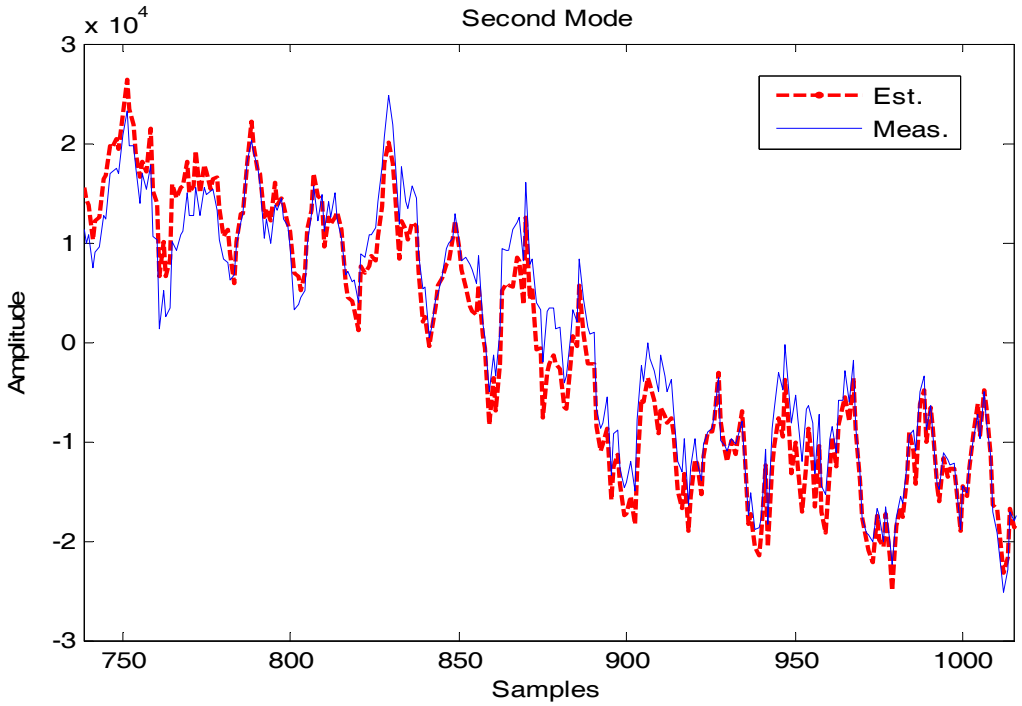

Figure 21. Zoom in on Second Mode Coefficient

XII. Geometric Interpretation: N-Width Approximation

Geometric interpretation of POD and balanced truncation in terms of optimizing the Kolmogorov, Gel'fand and linear *n*- widths of the corresponding compact operators is discussed. These *n*-widths quantify the inherent error generated in the information collecting stage of simulation or identification, due to lack of data and inaccurate measurements, and the representation error due to the loss of information in the information processing stage.

The eigenvalues λ_i's of $(T^*T)^{1/2}$ (or singular values of T) defined in (13), and the Hankel singular values σ_i's of Γ_G have a geometric interpretation in terms of the computation of the *n*-widths of compact operators T and Γ_G that are defined on Hilbert spaces $L^2([0,T))$ and $L^2(-\infty,0]$, respectively. In this section, we discuss the role of POD and balanced truncation in optimizing different *n*-widths defined in [61] (and references therein.)

In model reduction we are interested in approximation by finite dimensional models, and in particular, *n*-parameter affine models such as in POD and balanced truncation. This is related to the Kolmogorov *n*-width of $T(L^2(\Omega))$ into $L^2([0,T))$ as the optimization which characterizes the representation [61]

$$d_n(T(L^2(\Omega));L^2([0,T)) = \inf_{X_n} \sup_{\|f\|_2\le 1, f\in L^2(\Omega)} \inf_{g\in X_n} \|Tf-g\|_2 \qquad (163)$$

where X_n is an *n*-dimensional subspace of $L^2([0, T))$.

The Kolmogorov n-width measures the extent to which the space $L^2([0,T))$ can be approximated by *n*-dimensional subspaces of $T(L^2(\Omega))$, it is a measure of the "massivity" of $T(L^2(\Omega))$. It represents the minimum representation error of $T(L^2(\Omega))$ by the *n*-dimensional subspace X_n of $L^2([0, T))$. In other words, the Kolmogorov *n*-width quantifies the representation error due to inaccurate representation of the set $T(L^2(\Omega))$: It represents the loss of information in the information processing stage. The inverse function of $d_n(\bullet)$ was called the metric dimension function by Zames in 1976, and viewed as an appropriate measure of the metric complexity of uncertain systems. In our case it is the dimension of the smallest subspace whose elements can approximate arbitrary vectors of $T(L^2(\Omega))$ to a specified tolerance.

The *n*-width in the sense of Gel'fand, is defined as

$$d^n(T(L^2(\Omega)); L^2([0,T))) = \inf_{L^n} \sup_{\|f\|_2 \le 1,\, f \in L^n} \|Tf\|_2 \tag{164}$$

where the infimum is taken over all subspaces L^n of $T(L^2(\Omega))$ of codimension at most *n*. If

$$d^n(T(L^2(\Omega)); L^2([0,T)) = \sup\{\|f\|_2 : f \in T(L^2(\Omega)) \bigcap L^n\}$$

where L^n is a subspace of codimension at most *n*, then L^n is an optimal subspace for

$$d^n(T(L^2(\Omega)); L^2([0,T))$$

A subspace L^n is of codimension *n* if there exist *n* continuous linear functionals $\{f_i\}_{i=1}^n$ on $L^2([0, T))$ for which

$$L^n = \{g : g \in L^2(h),\, f_i(g) = 0, i = 1, 2, \ldots, n\} \tag{165}$$

The Gel'fand *n*-width characterizes the experimental complexity of the information collecting stage using simulation or identification. It is related to the inherent error due to lack of data and inaccurate measurements. The inverse of the Gel'fand n-width gives the least number of measurements needed to reduce the modeling uncertainty to a predetermined value.

The linear *n*-width is defined is defined by

$$\delta_n(T(L^2(\Omega)); L^2((-\infty, 0]) := \inf_{P_n} \sup_{\|\phi\|_2 \le 1, \phi \in L^2(\Omega)} \|T\phi - P_n\phi\|_2$$

where P_n is any continuous linear operator from $L^2(\Omega)$ into $L^2([0,T))$ of rank at most *n*.

Remark: Note similar definitions hold for the Hankel operator range $\Gamma_G(L^2[-\infty, 0))$.

The basic results of this section are the following theorems which tell us that the different *n* widths can be computed, and provide us with explicit optimal subspaces and operators.

Theorem: Let the operator *T* be defined as above, and let $\{\lambda_i\}$, $\{\alpha_i\}$, $\{\varphi_i\}$ be defined as above. Then

$$d_n(T(L^2(\Omega)); L^2((-\infty, 0])) = d^n(T(L^2(\Omega)); L^2((-\infty, 0])) = \delta_n(T(L^2(\Omega)); L^2((-\infty, 0])) = \lambda_{n+1}$$
$$n = 0, 1, 2, \cdots$$

Furthermore, the temporal coefficients $\{\alpha_i\}$ and POD basis $\{\varphi_i\}$ are optimal for the *n*-widths in the following sense:

i) The subspace spanned by the coefficients $\{\alpha_i\}$, is optimal for $X_n = \text{Span}\{\alpha_1, \cdots, \alpha_n\}$, is optimal for $d_n(T(L^2(\Omega)); L^2((-\infty, 0]))$.

ii) The subspace $L^n = \{\phi \in L^2(\Omega), < \phi, \varphi_i >_1 = 0, i = 1, 2, \cdots, n\}$ is optimal for $d^n(T(L^2(\Omega)); L^2((-\infty, 0]))$.

iii) The linear operator $P_n\phi = \sum_{i=1}^{n} < \phi, \varphi_i >_1 \varphi_i$ is optimal for $\delta_n(T(L^2(\Omega)); L^2((-\infty, 0]))$.

A similar Theorem holds for the Hankel operator Γ_G and is stated next

Theorem: Let the operator Γ_G be defined as above, and let $\{\sigma_i\}, \{\chi_i\}, \{\zeta_i\}$ be defined as above. Then

$$\begin{aligned} d_n(\Gamma_G(L^2((-\infty, 0])); L^2((0, \infty])) &= d^n(\Gamma_G(L^2((-\infty, 0])); L^2((0, \infty])) \\ &= \delta_n(\Gamma_G(L^2((-\infty, 0])); L^2((0, \infty])) \\ &= \lambda_{n+1}, \qquad n = 0, 1, 2, \cdots \end{aligned}$$

Furthermore, the temporal coefficients $\{\chi_i\}$ and POD basis $\{\zeta_i\}$ are optimal for the *n*-widths in the following sense:

i) The subspace spanned by the coefficients $\{\zeta_i\}$, $X_n = \text{Span}\{\zeta_1, \cdots, \zeta_n\}$, is optimal for for $d_n(\Gamma_G(L^2((-\infty, 0])); L^2((0, \infty]))$.

ii) The subspace $L^n = \{\chi \in L^2(-\infty, 0], \int_{-\infty}^{0} \chi(\tau)\chi_i(\tau) = 0, i = 1, 2, \cdots, n\}$ is optimal for $d^n(\Gamma_G(L^2((-\infty, 0])); L^2((0, \infty]))$.

iii) The linear operator $Q_n\phi = \sum_{i=1}^{n} \int_{-\infty}^{0} \phi(\tau)\chi_i(\tau) d\tau \chi_i$ is optimal for $\delta_n(\Gamma_G(L^2(-\infty, 0]); L^2[0, \infty))$.

POD may fail to capture the nonlinear degrees of freedom in nonlinear PDEs, in particular for navier-Stokes equations with Reynolds numbers in the thousands, since it assumes that data belong to a linear space and therefore relies on the Euclidean distance as the metric to minimize. However, snapshots generated by nonlinear PDEs belong to manifolds for which the geodesics, when they exist, do not correspond in general to the Euclidean distance. A geodesic is a curve that is locally the shortest path between two points. In this next section, we propose a model reduction method which generalizes POD to nonlinear fluid flows corresponding to manifolds which have a differentiable structure at each of their points. The algorithm is applied to a prototype nonlinear turbulent flow governed by the Navier-Stokes equation.

XIII. Nonlinear Proper Orthogonal Decomposition (POD): Auto-Associative Models

Nonlinear POD is inspired from auto-associative models that have been introduced as a new tool that deals with nonlinear data. Such models rely on successive approximations of a dataset by manifolds of increasing dimensions. In this paper, auto-associative models are proposed as candidates to generalize POD to nonlinear systems. These models are dedicated to the approximation of datasets by manifolds [62]. Let us introduce definitions

A function $F^d : \mathbb{R}^p \to \mathbb{R}^p$ is a *d*-dimensional auto-associative function if there exist *d* unit orthogonal vectors a^k, called proper directions, and *d* continuously differentiable functions $s^k : \mathbb{R} \to \mathbb{R}^p$, called regression functions, such that [62]

$$P_{a^j} \circ s^k = \delta_{j,k} Id_{\mathbb{R}} \text{ for all } 1 \le j \le k \le d \tag{166}$$

where $\delta_{j,k}$ is the Kronecker symbol and for each unit vector $a \in \mathbb{R}^p$, we denote by $P_a(\bullet) = \langle a, \bullet \rangle$ the linear projection from $\mathbb{R}^p$ to $\mathbb{R}$. Also, for all sets E, the identity function $E \to E$ is denoted by Id_E [62]. Define

$$\begin{aligned} F^d &= (Id_{\mathbb{R}^p} - s^d \circ P_{a^d}) \circ \cdots \circ (Id_{\mathbb{R}^p} - s^1 \circ P_{a^1}) \\ &= \coprod_{k=d}^{1} (Id_{\mathbb{R}^p} - s^k \circ P_{a^k}) \end{aligned} \tag{167}$$

The equation $F^d(x) = 0,\ x \in \mathbb{R}^p$ defines a differentiable d-dimensional manifold of $\mathbb{R}^p$ [63]. Thus, the equation $F^d(x) = 0$ defines a space in which every point has a neighborhood which resembles the Euclidean space $\mathbb{R}^d$, but in which the global structure may be more complicated. As an example, on a 1-dimensional manifold, every point has a neighborhood that resembles a line. In a 2-manifold, every point has a neighborhood that looks like a plane.

Let X be a square integrable vector function of $\mathbb{R}^p$. X represents snapshots. For an auto-associative function F^d, consider $\varepsilon = F^d(X)$ where in this context, $\|\varepsilon\|_2^2$ is called the residual error. PDE Snapshots X are approximated by the manifold $F^d(x) = 0,\ x \in \mathbb{R}^p$ and $\|\varepsilon\|_2^2$ represents the (squared) norm of X outside the manifold.

Note that such vector X always satisfies a 0-dimensional auto-associative model with $F^0 = Id_{\mathbb{R}^p}$ and $\|\varepsilon\|_2^2 = \|X\|_2^2$. Similarly, X always satisfies a *p*-dimensional auto-associative model with $F^p = 0$ and $\|\varepsilon\|_2^2 = 0$. In practice, it is important to find a balance between these two extreme cases by constructing a *d*-dimensional model with $d \ll p$ and $\|\varepsilon\|_2^2 \ll \|X\|_2^2$.

For instance, in the case where the autocorrelation $\sum$ of X is of rank *d*, then X is located on a *d*-dimensional linear subspace defined by the equation $F_{POD}^d(x) = 0$ with

$$F_{POD}^d(x) = x - \sum_{k=1}^{d} P_{a^k}(x) a^k \tag{168}$$

where a^k, $k=1,\cdots,d$ are the eigenvectors of $\sum$ associated to the positive eigenvalues. Equation (168) can be rewritten as $F^d(x)=0$, where F^d is a d-dimensional auto-associative function with linear regression functions $a^k(t),\ k=1,\cdots,d$. Moreover, we have $\|\varepsilon\|_2^2=0$.

Since (168) is the model produced by a POD, it straightforwardly follows that POD is a special (linear) case of auto-associative models. In the next section, we show an algorithm to build auto-associative models with non-necessarily linear regression functions, small dimension and small residual error.

A. Projection Algorithm

Given a unit vector $a\in\mathbb{R}^p$, an index $I:\mathbb{R}\to\mathbb{R}$ is a functional measure the interest of the projection $P_a(X)$ with a non negative real number. This depends on the considered data analysis problem. For instance, a possible choice of I is the projected squared L_2 norm $I\circ P_a(\bullet)=\|P_a(\bullet)\|^2$. So, the maximization of $I\circ P_a(X)$ with respect to a yields the most interesting direction for this given criteria [64].

Let $d\in\{0,\cdots,p\}$, the projection algorithm applies the following iteratively: computation of the axes, projection, regression and update [64][65].

Algorithm: Define $R^0=X$
For $k=1,\cdots,d$:

1) Determine $a^k=\arg\max_{x\in\mathbb{R}^p} I\circ P_x(R^{k-1})$ such that $\|x\|_2=1, P_{a^j}(x)=0, 1\le j<k$
2) Compute $Y^k=P_{a^k}(R^{k-1})$
3) Estimate $s^k(t)_{Y^k=t}=R^{k-1}$
4) Compute $R^k=R^{k-1}-s^k(Y^k)$

Step 1 computes an axis orthogonal to the previous ones and maximizes a given index I. Step 2 projects the residuals on this axis to determine the proper variables Y^k, and step 3 estimates of the regression function of Y^k best approximating the residuals. Finally Step 4 updates the residuals.

In the next section, the algorithm is applied to a prototype nonlinear turbulent flow governed by the Navier-Stokes equation.

B. Full Order System

To test the algorithm, our data is a numerical finite element solution of Navier Stokes equations that describes the dynamics of an incompressible turbulent flow. General Navier -Stokes equations are of the following form [66]

$$\partial_t \rho + \nabla \cdot [pv] = 0, \tag{169}$$

$$\partial_t (\rho v) + \rho v \cdot \nabla v - \nabla \cdot \left[\mu \nabla v + \frac{1}{3} \mu \nabla \cdot vI \right] + \nabla p_{tot} = \rho f \tag{170}$$

$$\partial_t (c_p \rho T) + c_p \rho v \nabla T - \nabla \cdot [\lambda \nabla T] = h \tag{171}$$

where v is the velocity, ρ the density, p_{tot} the total pressure, and T the temperature of the fluid occupying a two- or three-dimensional region . The parameters $\mu > 0$ (dynamic viscosity), $c_p > 0$ (heat capacity) and $\lambda > 0$ (heat conductivity) characterize the properties of the fluid. The volume force f and the heat source h are explicitly given.

In temperature-driven flows, h may implicitly depend on the temperature and further quantities describing heat release, as for example by chemical reactions. For simplicity, we assume an incompressible flow (i.e. ρ is constant), then we have:

$$\nabla \bullet v = 0$$

In this model, we consider as the primal unknowns the velocity v , the pressure $p = p_{tot}$, and the temperature T . For most parts of the discussion, the flow is assumed to be isothermal, so that the energy equation decouples from the momentum and continuity equations, and the temperature only enters through the viscosity parameter. The system is closed by imposing appropriate initial and boundary conditions for the flow variables

$$\begin{aligned} v|_{t=0} &= v^0, \\ v|_{\Gamma_{rigid}} &= 0, \\ v|_{\Gamma_{in}} &= v^{in}, \\ \left(\mu \partial_n v + pn \right)|_{\Gamma_{out}} &= 0 \end{aligned}$$

and corresponding ones for the temperature, where Γ_{rigid}, Γ_{in} and Γ_{out} are the rigid part, the inflow part and the outflow part of the boundary $\partial\Omega$, respectively.

Assuming the isothermal case, i.e. $\rho_0 = 1$, the Navier Stokes system can be written as [66]:

$$\partial_t v + v \bullet \nabla v - k \nabla v + \nabla p = f, \quad \nabla \bullet v = 0 \tag{171}$$

with the kinematic viscosity parameter $k = \frac{\mu}{\rho_0}$. In this formulation the domain Ω may be taken two or three dimensional according to the particular requirements of the simulation.

C. Weak Formulation

Taking the inner product of both sides of (171) with the i-th nonlinear POD mode Y^i and utilizing Green's identities results in the weak formulation in a similar fashion as in [12] to get:

$$\langle \partial_t v, \varphi \rangle + \langle \nabla v, \nabla \varphi \rangle + \langle v.\nabla v, \varphi \rangle - \langle p, \nabla . v \rangle = \langle f, \varphi \rangle \tag{172}$$

re $\langle \bullet, \bullet \rangle$ denote the inner product in $L^2(\Omega)$, and smooth $\varphi \in L^2(\Omega)$.

The problem is numerically solved using Comsol Multiphysics [66]. Figure 24 shows the problem geometry, boundary conditions and the full order velocity solution. Wortmann FX 60-100 airfoil is used. The finite element discretization results in 10029 degree of freedom, other parameters are as follows:

Density: $\rho = 1 kg / m^3$

Dynamic Viscosity: $\mu = 0.001 Pascal.\sec$

Reynolds Number: $R_e = 1000.$

The full order fluid flow model is represented in Figure 22. The reduced order model has 50 states and is represented in Figure 23. Both Figures show that good agreement between both flows. We are currently generalizing the method to Reynolds numbers in the tens of thousands.

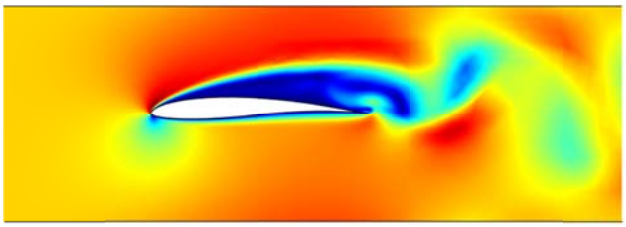

Figure 22. Full Order Finite Element Solution

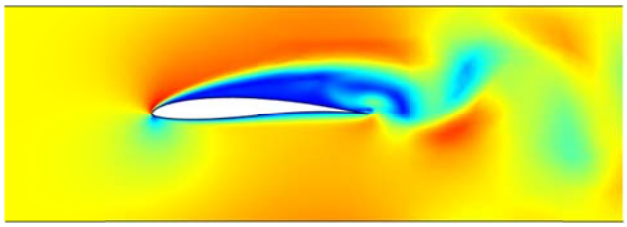

Figure 23. Reduced Order Model

XIV. Conclusion

In this project, model reduction algorithms and control design approaches for aerodynamic flows were developed. The goal of this research is eventually to develop a methodology for feedback control of fluid flows modeled by Navier-Stokes equations. The proposed work places an emphasis upon aerodynamic control. For the case of boundary control, the development of reduced models has been an open problem. For many Air Force applications of practical interest, such as feedback control of the air flow over an airplane wing, boundary actuation is a requirement. These applications require actuation to be located on the surface if they are to be implemented in hardware in the physical system. Most reduced modeling efforts have either been concerned with the case of control action via a body force or have approximated boundary actuation by a body force on the domain interior. In this project, we have developed a

methodology which extracts boundary conditions in reduced order POD and finite difference models. For the most part, this method utilizes POD and finite difference bases in combination with a weak formulation of the Galerkin projection to construct models where boundary control input appears explicitly. Special care is taken when POD is used for the development of feedback control laws. In particular, construction of a POD basis capable of spanning the baseline solution, as well as dynamics introduced by boundary actuation has been addressed using a method called split POD.

Tools borrowed from the theory of operators were used to show that POD and balanced truncation are optimal in a precise sense. Optimality is quantified in terms of optimal approximations by lower rank Hilbert-Schmidt (integral) operators in Hilbert-Schmidt norms. The difference in the two model reduction techniques lies in the fact, that the optimizations occur in different integral operators defined on different L^2 spaces. However, both optimal approximations are posed in Hilbert operator spaces allowing for the optimal approximations to be computed explicitly.

Model estimation and identification of the POD modes for a turbulent flow over the NACA 4412 airfoil is developed. The model is constructed from PIV experimental measurements obtained from the flow control group at Syracuse University. The dynamics of the flow are captured using a linear stochastic state-space model. Estimation and identification algorithms solely from wing surface pressure measurement data are developed. These algorithms are based on combining the KF with the EM algorithm that estimate and identify recursively the state of the flow and its parameters, respectively. Numerical results are provided to evaluate the accuracy of the proposed algorithms.

Empirical balanced truncation and Hankel norm model reduction have been considered in conjunction with POD as an approach for deriving reduced-order models. Like POD, both are based on simulation/experimental data and can be implemented via standard matrix computations. Improvements to the scheme originally proposed in [5][23] have been presented that lead to reduced data requirements that may become significant for applications such as aerodynamic flow control. Essentially, the balancing transformation is constructed via Markov parameters that can be identified from measurements collected in a single experiment/ simulation. The approach has been applied with favorable results to nonlinear convection governed by the 2D Burgers' equation, a partial differential equation in two spatial dimensions that possesses features comparable to the Navier-Stokes equations governing fluid flow. A H^∞ feedback flow controller was designed based on the empirical reduced model to achieve flow tracking. The closed-loop on the full order model shows good flow tracking performance.

Geometric interpretation of POD and balanced truncation in terms of optimizing the Kolmogorov, Gel'fand and linear *n*-widths is discussed. These *n*-widths quantify the inherent and representation errors generated in the information collecting and processing stages in simulation or identification. To the best of our knowledge this is the first time that model reduction and metric complexity theory with the notion of n-width are related to each other in an explicit way.

A novel model reduction method which generalizes POD to nonlinear PDEs with solutions belonging to manifolds which have (approximately) a differentiable structure at each of their points. Conventional POD is widely used to reduce the order of high order models of nonlinear system but it fails with systems of high nonlinearity because the projection is done to a linear Euclidean space. Non-linear POD proposed here solves this limitation using a projection on the manifold constructed from the input data. In future work we plan to improve and test our algorithm on systems with higher nonlinearities by increasing the Reynolds numbers of turbulent flows.

Acknowledgment/Disclaimer

This work was sponsored (in part) by the Air Force Office of Scientific Research, USAF, under grant/contract number AF-FA9550-08-1-0450. The views and conclusions contained herein are those of the author and should not be interpreted as necessarily representing the official policies or endorsements, either expressed or implied, of the Air Force Office of Scientific Research or the U.S. Government.

References

[1] M. Samimy, M. Debiasi, E. Caraballo, A. Serrani, X. Yuan, J. Little and J. H. Myatt, Feedback control of subsonic cavity flows using reduced-order models, J. Fluid Mech. (2007), vol. 579, pp. 315-346.
[2] Willcox, K. and Peraire, J., Balanced Model Reduction via the Proper Orthogonal Decomposition, AIAA, Vol. 40, No. 11, November 2002, pp. 2323-2330.
[3] Djouadi, S.M., R.C. Camphouse and J.H. Myatt, Optimal Order Reduction for the Two-Dimensional Burgers' Equation, Proceedings of the IEEE Conference on Decision and Control, pp. 3507 – 3512, December 2007.
[4] Ilak, M. and Rowley, C. W., "Reduced-Order Modeling of Channel Flow Using Traveling POD and Balanced POD", AIAA Flow Control Conference, pp. 1-11, 5-8 June 2006.
[5] Lawrence, D. A., "Empirical Model Reduction for Active Closed-Loop Flow Control", Final Report for Faculty Summer Research Opportunity, ARL Ohio, 2004.
[6] Leibfritx, F. and Volkwein, S. , "Numerical feedback controller design for PDE systems using model reduction: techniques and case studies". Real-Time PDE-Constrained Optimization, SIAM, 2006.
[7] Rowley, C. W., Colonius, T., Murray, R. M., "Model reduction for compressible flows using POD and Galerkin projection." Physica D, 189 (2004), pages 115-129.
[8] Carlson, H., Glauser, M., Higuchi, H., and Young, M., POD Based Experimental Flow Control on a NACA-4412 Airfoil, AIAA Paper 2004-0575, January 2004.
[9] Carlson, H., Glauser, M., and Roveda, R., Models for Controlling Airfoil Lift and Drag, AIAA Paper 2004-0579, January 2004.
[10] Cohen, K., Siegel, S., McLaughlin, T., and Myatt, J., Proper Orthogonal Decomposition Modeling of a Controlled Ginzburg-Landau Cylinder Wake Model, AIAA Paper 2003-2405, January 2003.
[11] Camphouse, Chris R. and James H. Myatt, "Reduced Order Modelling and Boundary Feedback Control of Nonlinear Convection", 2005 AIAA Guidance, Navigation, and Control Conference, Paper AIAA-2005-5844, 2005.

[12] R.C. Camphouse, S.M. Djouadi and J.H. Myatt, Feedback Control for Aerodynamics, AFRL-VA-WP-TP-2006-348, September 2006.
[13] Graham, W. R., Peraire, J., Tang, K. Y., "Optimal Control of Vortex Shedding Using Low-Order Models. Part I—Open-Loop Model Development," International Journal for Numerical Methods in Engineering, 44, pp. 945-972, 1999.
[14] Banks, H., Del Rosario, R., and Smith, R., Reduced Order Model Feedback Control Design: Numerical Implantation in a Thin Shell Model, Technical Report CRSC-TR98-27, Center for Research in Scientific Computation, North Carolina State University, June, 1998.
[15] Caraballo, E., Samimy, M., and DeBonis, J., Low Dimensional Modeling of Flow for Closed-Loop Flow Control," AIAA Paper 2003-0059, January 2003.
[16] Rugh, W. J., Linear System Theory, Prentice Hall, Second Edition, 1996.
[17] Sohr, H., The Navier-Stokes Equations: An Elementary Functional Analytic Approach, Birkhauser Verlag, 2001.
[18] Zhou, K., Doyle, J.C., and Glover, K., Robust and Optimal Control, Prentice Hall, 1996.
[19] Zhou, K. and Doyle, J. C., Essentials of Robust Control, Prentice Hall, 1998
[20] Defant, A and K. Floret, Tensor Norms and Operator Ideals, Elsevier Science, 1993.
[21] Moore, B. C., "Principal Component Analysis in Linear Systems: Controllability, Observability, and Model Reduction," Trans. on Automatic Control, pp. 17-32, 1981.
[22] Condon, M. and Ivanov, R., "Empirical Balanced Truncation of Nonlinear Systems," Journal of Nonlinear Science. Vol. 14: pp. 405-414, 2004.
[23] Hahn, J. and Edgar, T. F., "Reduction of nonlinear models using balancing of empirical Gramians and Galerkin projections," Proceedings of the American Control Conference, pp. 2864-2868, June 2000.
[24] Antoulas, C.A., "Approximation of Large-Scale Dynamical Systems," Advances in Design and Control, SIAM, 2006. Scientific Computation, North Carolina State University, June, 1998.
[25] Sreeram, V., "Frequency Response Error Bounds for Time-Weighted Balanced Truncation," Proceedings of the 41st IEEE Conference on Decision and control, pp. 3330 – 3331, December 2002.
[26] J. Lumley, The Structures of Inhomogeneous Turbulent Flow, Atmospheric Turbulence and Radio Wave Propagation, edited by A. M. Yaglom and V.I. Tatarski, Nauka, Moscow, pp. 166-178, 1967.
[27] Holmes, P., Lumley, J., and Berkooz, G., Turbulence, Coherent Structures, Dynamical Systems and Symmetry, Cambridge University Press, New York, 1996.
[28] Berkooz, G., Holmes, P., and Lumley, J., The Proper Orthogonal Decomposition in the Analysis of Turbulent Flows, Annual Review of Fluid Mechanics, Vol. 25, 1993, pp. 539-575.
[29] J. Borggaard, Optimal Reduced-Order Modeling for Nonlinear Distributed Parameter Systems, Proceedings of the American Control Conference, Minneapolis, pp. 1150-1154, 2006.
[30] L. Mirsky, Symmetric Gauge Functions and Unitarily Invariant Norms, Quart. J. Math (2), 11 (1960), pp. 50-59.
[31] F. Riesz and B.Sz.-Nagy, Functional Analysis, Dover, 1990.
[32] Schatten R. Norm Ideals of Completely Continuous Operators, Springer-Verlag, Berlin, Gottingen, Heidelberg, 1960.
[33] L.M. Silverman and M. Bettayeb, Optimal Approximation of Linear Systems, Proceedings of the American Control Conference, 1981.

[34] K. Glover, R.F. Curtain and R. Partington, Realisation and Approximation of Linear Infinite Dimensional Systems with Erroe Bounds, SIAM J. Control and Optiz., vol. 26, No. 4, (1988), pp. 863-898.
[35] Karhunen, K., "Zur Spektraltheorie Stochastischer Prozesse", Annales Academiæ Scientiarum Fennicæ, 1946.
[36] Loéve, M. M., Probability Theory, Princeton, NJ: VanNostrand, 1955.
[37] Hotelling, H., "Analysis of a Complex of Statistical Variables Into Principal Components", Journal of Educational Psychology, pp. 417-441, 1933.
[38] Atwell, J. A., Borggaard, J. T., King, B. B., "Reduced Order Controllers For Burgers' Equation With A Nonlinear Observer", Int. J. Appl. Math. Compu-tational Science., 2001, Vol.11, No.6, pgs. 1311-1330.
[39] Efe, M. O. And Ozbay H., "Proper Orthogonal Decomposition for Reduced Order Modeling: 2D Heat Flow", IEEE Conf. on Decision and Control, 2003.
[40] Rowley, C. W., Colonius, T., Murray, R. M., "Model reduction for compressible flows using POD and Galerkin projection." Physica D, 189 (2004), pages 115-129.
[41] Graham, W. R., Peraire, J., Tang, K. Y., "Optimal Control of Vortex Shedding Using Low-Order Models. Part I—Open-Loop Model Development," International Journal for Numerical Methods in Engineering, 44, pp. 945-972, 1999.
[42] Rowley, C. W., Colonius, T., Murray, R. M., "Model reduction for compressible flows using POD and Galerkin projection." Physica D, 189 (2004), pages 115-129
[43] Sirovich, L., "Turbulence and the Dynamics of Coherent Structures, Parts I-III," Quarterly Journal of Applied Mathematics, Volume 45, Brown University, Rhode Island, pp. 561-590, 1987.
[44] J. Juang, Applied System Identification, Prentice Hall, 1994. 121-230.
[45] S.M. Djouadi, R.C. Camphouse, and J.H. Myatt, Empirical Reduced-Order Modeling for Boundary Feedback Flow Control, Journal of Control Science and Engineering Volume 2008 (2008), Article ID 154956, 11 pages.
[46] S. M. Djouadi, On the Optimality of the Proper Orthogonal Decomposition and Balanced Truncation, Proceedings of the 47th IEEE Conference on Decision and Control, Cancun, Mexico, December 2008, pp. 4221- 4226.
[47] Rugh, W. J., Linear System Theory, Prentice Hall, Second Edition, 1996.
[48] Caicedo, J. M., Dyke, S. J., and Jonson, E. A., "Natural Excitation Technique and Eigensystem Realization Algorithm for Phase 1 of the IASC-ASCE Benchmark Problem: Simulated Data", Journal of Engineering Mechanics, January 2004, pgs. 49-60.
[49] Lall, S., Marsden, J. E., Glavaski, S. "A Subspace Approach to Balanced Truncation for Model Reduction of Nonlinear Control Systems", International Journal of Robust and Nonlinear Control, 2002; No. 12, pages 519-535.
[50] Lawrence, D. A., Myatt, J. H., and Camphouse, R. C., "On Model Reduction via Empirical Balanced Truncation", American Control Conference, June, 2005.
[51] Mathworks, "Partial Differential Equations Toolbox Help". [Available Online: http://www.mathworks.com/access/helpdesk/help/toolbox/pde/].
[52] Graham, W. R., Peraire, J., Tang, K. Y., "Optimal Control of Vortex Shedding Using Low-Order Models. Part I—Open-Loop Model Development," International Journal for Numerical Methods in Engineering, 44, pp. 945-972, 1999.

[53] Hahn, J. and Edgar, T. F., "Reduction of nonlinear models using balancing of empirical Gramians and Galerkin projections," Proceedings of the American Control Conference, June 2000.
[54] Glover, K., "All Optimal Hankel-norm Approximations of Linear Multivariable Systems and Their L – Error Bounds," International Journal of Control, vol. 39, pp. 1115-1193, 1984.
[55] Pinier, J.M. Ausseur, M.N. Glauser, and Higuchi, H., "Proportional closed-loop feedback control of flow separation," *AIAA Journal*, Vol. 45, No. 1, pp. 181–190, 2007.
[56] Glauser, M.N., Higuchi, H., Ausseur, J., and Pinier, J., "Feedback control of separated flows," *2nd AIAA Flow Control Conference*, 2004. AIAA Paper 2004-2521.
[57] Ausseur, J.M., Pinier, J.T., and Glauser, M. N., "Estimation Techniques in a Turbulent Flow Field," *37th AIAA Fluid Dynamics Conference and Exhibit,* 25 - 28 June 2007, Miami, FL, paper AIAA 2007-3975.
[58] C.D. Charalambous and A. Logothetis, "Maximum-likelihood parameter estimation from incomplete data via the sensitivity equations: The continuous-time case", IEEE Transaction on Automatic Control, vol. 45, no. 5, pp. 928-934, May 2000.
[59] G. Bishop and G. Welch, An introduction to the Kalman filters, University of North Carolina, 2001.
[60] Chung, T. J., Computational Fluid Dynamics, Cambridge University Press, 2002.
[61] A. Pinkus, n-Widths in Approximation Theory, Springer-Verlag, 1985.
[62] Girard and Iovleff Principal Manifolds for Data Visualisation and Dimension Reduction pp 205-222.
[63] Girard, S.: A nonlinear PCA based on manifold approximation. Computational Statistics, 15 (2), 145–167 (2000).
[64] Huber, P.J.: Projection pursuit. The Annals of Statistics, 13 (2), 435–475 (1985).
[65] Jones, M.C. and Sibson R.: What is projection pursuit? Journal of the Royal Statistical Society A, 150, 1–36 (1987).
[66] R. Becker (1995), An Adaptive Finite Element Method for the Incompressible Navier-Stokes Equations on Time-Dependent Domains, Doctor Thesis, Preprint 95-44, SFB 359, Nov. 1995, University of Heidelberg.
[67] S.M. Djouadi, R.C. Camphouse, and J.H. Myatt, Empirical Reduced-Order Modeling for Boundary Feedback Flow Control, Journal of Control Science and Engineering Volume 2008 (2008), Article ID 154956, 11 pages.

Personnel Supported During Duration of Grant

Ms. Tasha Fernandez	Graduate student, University of Tennessee, Knoxville
Mr. Samir Sahyoun	Graduate student, University of Tennessee, Knoxville
Dr. Viktor Chupryna	Postdoc, University of Tennessee, Knoxville
Dr. Seddik M. Djouadi	Associate Professor, University of Tennessee, Knoxville

Publications

S.M. Djouadi, R.C. Camphouse and J.H. Myatt, "Optimality of the Proper Orthogonal Decomposition and Balanced Model Reduction with Application to a Nonlinear Convective Flow", IEEE Transactions on Automatic Control, submitted.

S.M. Djouadi, "On the Connection between Balanced Proper Orthogonal Decomposition, Balanced Truncation, and Metric Complexity Theory", IEEE Transactions on Automatic Control, submitted.

S.M. Djouadi and M.M. Olama, "Estimation and Identification of an Airfoil Flow Model Based on Raw Pressure Surface Sensors Measurements", submitted to AIAA journal.

T. Fernandez and S.M. Djouadi, Analytical Computation of POD Modes and Metric Complexity Metrics for the Heat Equation Subject to Boundary Control, submitted to the Journal of Guidance, Control, and Dynamics.

T. Fernandez, S. M. Djouadi and J. Foster, Empirical Hankel Norm Model Reduction with Application to a Prototype Nonlinear Convective Flow, submitted to the Journal of Control Engineering.

S. Sahyoun and S.M. Djouadi, Nonlinear Proper Orthogonal Decomposition for Fluid Flows Model, NSF CMMI Grantee Conference, Atlanta, GA, pp. 166-171, January 4-7, 2011.

S.M. Djouadi and S. Sahyoun, "On a Generalization of the Proper Orthogonal decomposition and Optimal Construction of Reduced Order Models", submitted to the IEEE Conference on Decision and Control, to be held in Orlando, FL, in December 2011. (Invited)

S. Sahyoun and S.M. Djouadi, "Nonlinear Model Reduction for Fluid Flows", accepted for publication in the American Control conference to be held in San Francisco, June 2011. (Invited)

Tasha Fernandez, "Analytical Computation of Proper Orthogonal Decomposition Modes and n-Width Approximations for the Heat Equation with Boundary Control," M.Sc. thesis, Department of Electrical Engineering and Computer Science, University of Tennessee, August, 2010.

S.M. Djouadi, "On the Connection between Balanced Proper Orthogonal Decomposition, Balanced Truncation, and Metric Complexity Theory for Infinite Dimensional Systems", Proceedings of the Conference of the American Control Conference (ACC), pp. 4911 - 4916, June 2010. (Invited)

T. Fernandez, S.M. Djouadi and J. Foster, "Empirical Hankel Norm Model Reduction with Application to a Prototype Nonlinear Convective Flow", Proceedings of the Conference of the American Control Conference (ACC), pp. 3771 - 3776, June 2010.

T. Fernandez, S.M. Djouadi and R.C. Camphouse, "Analytical Computation of Proper Orthogonal Decomposition Modes and n-Width Approximations for the Heat Equation with Boundary Control". The Proceedings of the IEEE Conference on Decision and Control, Atlanta, GA, December 15-17, 2010, pp. 2191-2196. (Invited)

M. Dkhiri, "Finite Element Galerkin Approach to the Two-Dimensional Burgers' Equation", (2009). M.Sc. thesis, Department of Electrical Engineering and Computer Science, the University of Tennessee, April 2009.

S. M. Djouadi, R. Chris Camphouse, and James H. Myatt, Empirical Reduced-Order Modeling for Boundary Feedback Flow Control, Journal of Control Science and Engineering Volume 2008 (2008), Article ID 154956, 11 pages.doi:10.1155/2008/154956.

S.M. Djouadi, On the Optimality of the Proper Orthogonal Decomposition and Balanced Truncation, Proceedings of the 47th IEEE Conference on Decision and Control, Cancun, Mexico, December 2008, pp. 4221- 4226.

Presentations

S.M. Djouadi, Nonlinear Proper Orthogonal Decomposition for Fluid Flows Model, NSF CMMI Grantee Conference, Atlanta, GA, January 4-7, 2011.

S.M. Djouadi , "Analytical Computation of Proper Orthogonal Decomposition Modes and n-Width Approximations for the Heat Equation with Boundary Control". The IEEE Conference on Decision and Control, held in Atlanta, December 15-17. (Invited)

S.M. Djouadi, "On the Connection between Model Reduction and n-Widths Approximation", (2010). SIAM Conference on Control and Its Applications, Pittsburgh, PA July 12-16, 2010. (Invited)

S.M. Djouadi, "On the Connection Between Balanced Proper Orthogonal Decomposition, Balanced Truncation, and Metric Complexity Theory for Infinite Dimensional Systems, the American Control Conference (ACC), held in Baltimore, MD, June 2010. (Invited)

T. Fernandez, "Empirical Hankel Norm Model Reduction with Application to a Prototype Nonlinear Convective Flow", the American Control Conference (ACC), held in Baltimore, MD, June 2010.

Seddik M. Djouadi, "Optimal Model Reduction with Application to Nonlinear Convection", (2009). Conference Proceedings, Published Bibliography: SIAM Conference on Control and Its Applications, July 6th-8th 2009 in Denver, CO. (Invited)

Seddik M. Djouadi, On the Optimality of the Proper Orthogonal Decomposition and Balanced Truncation, Proceedings of the 47th IEEE Conference on Decision and Control, Cancun, Mexico, December 2008.

AFRL Point of Contact

James H. Myatt, AFRL/VACA, WPAFB, OH, Phone: (937) 255-8498. Met at WPAFB, May 22, 2006.

Transitions

None.